Article

Current Biology

Astroglial Calcium Signaling Encodes Sleep Need in *Drosophila*

Highlights

- $Ca2^{+}$ dynamics within astrocytes correlate with sleep need in *Drosophila*
- Manipulating astrocyte Ca^{2+} signaling alters sleep behavior
- A monoaminergic receptor is required in astrocytes for homeostatic control of sleep
- Astrocytic Spätzle conveys sleep need to a homeostatic sleep circuit via Toll

Authors

Ian D. Blum, Mehmet F. Keleş, El-Sayed Baz, ..., Masashi Tabuchi, Sha Liu, Mark N. Wu

Correspondence

sha.liu@kuleuven.vib.be (S.L.), marknwu@jhmi.edu (M.N.W.)

In Brief

How sleep need is sensed, integrated, and conveyed to downstream sleep circuits is poorly understood. Blum et al. find that Ca^{2+} transients in fly astrocytes correlate with time spent awake and identify molecular and circuit mechanisms underlying the generation, amplification, and transmission of these signals encoding sleep need.

Blum et al., 2021, Current Biology *31*, 150–162
January 11, 2021
https://doi.org/10.1016/j.cub.2020.10.012

CellPress

CellPress

Current Biology

Article

Astroglial Calcium Signaling Encodes Sleep Need in *Drosophila*

Ian D. Blum,[1,6] Mehmet F. Keleş,[1,6] El-Sayed Baz,[2] Emily Han,[3] Kristen Park,[1] Skylar Luu,[1] Habon Issa,[1,4] Matt Brown,[3] Margaret C.W. Ho,[1] Masashi Tabuchi,[1,5] Sha Liu,[2,*] and Mark N. Wu[1,3,7,*]

[1]Department of Neurology, Johns Hopkins University, Baltimore, MD 21205, USA

[2]VIB Center for Brain and Disease Research and Department of Neurosciences, KU Leuven, Leuven 3000, Belgium

[3]Solomon H. Snyder Department of Neuroscience, Johns Hopkins University, Baltimore, MD 21205, USA

[4]Present address: Sackler Institute of Graduate Biomedical Sciences, New York University, New York, NY 10016, USA

[5]Present address: Department of Neurosciences, Case Western Reserve University, Cleveland, OH 44106, USA

[6]These authors contributed equally

[7]Lead Contact

*Correspondence: sha.liu@kuleuven.vib.be (S.L.), marknwu@jhmi.edu (M.N.W.)

https://doi.org/10.1016/j.cub.2020.10.012

SUMMARY

Sleep is under homeostatic control, whereby increasing wakefulness generates sleep need and triggers sleep drive. However, the molecular and cellular pathways by which sleep need is encoded are poorly understood. In addition, the mechanisms underlying both how and when sleep need is transformed to sleep drive are unknown. Here, using *ex vivo* and *in vivo* imaging, we show in *Drosophila* that astroglial Ca^{2+} signaling increases with sleep need. We demonstrate that this signaling is dependent on a specific L-type Ca^{2+} channel and is necessary for homeostatic sleep rebound. Thermogenetically increasing Ca^{2+} in astrocytes induces persistent sleep behavior, and we exploit this phenotype to conduct a genetic screen for genes required for the homeostatic regulation of sleep. From this large-scale screen, we identify TyrRII, a monoaminergic receptor required in astrocytes for sleep homeostasis. TyrRII levels rise following sleep deprivation in a Ca^{2+}-dependent manner, promoting further increases in astrocytic Ca^{2+} and resulting in a positive-feedback loop. Moreover, our findings suggest that astrocytes then transmit this sleep need to a sleep drive circuit by upregulating and releasing the interleukin-1 analog Spätzle, which then acts on Toll receptors on R5 neurons. These findings define astroglial Ca^{2+} signaling mechanisms encoding sleep need and reveal dynamic properties of the sleep homeostatic control system.

INTRODUCTION

The regulation of sleep by homeostatic forces is one of its defining features, and yet how sleep need is sensed and transduced into sleep drive remains poorly understood. The analysis of sleep homeostasis can be guided by engineering control principles that posit that homeostatic systems comprise at least 3 components: a sensor that receives information about the state variable; an integrator that computes the difference between this state variable and a setpoint; and a downstream effector that responds to the integrator and directly manipulates the state variable.[1] Although the signal(s) detected by "sleep sensors" remain debated, there is compelling evidence that a key stimulus for triggering sleep need is neuronal activity.[2,3] For instance, studies in rodents and humans have demonstrated that tasks that activate specific regions in the brain will then locally promote an increase in the amplitude of electroencephalographic slow-wave activity, an established marker of sleep need.[4–6]

More than a century ago, Cajal proposed that astrocytes, a subtype of glial cells, modulate neural connectivity across the sleep/wake cycle.[7] Since that time, emerging data have suggested that astrocytes play a key role in the regulation of sleep.[8–11] However, whether and how astrocytes sense and discharge sleep need is enigmatic. A number of special features of astrocytes make them well suited for serving as "sensors" of sleep need. Astrocytes effectively tile the entire brain, and their processes form an intimate network around synapses and locally sample neural activity.[12–15] In addition, Ca^{2+} signaling plays an important role in astrocyte function, and modulation of intracellular Ca^{2+} levels is a broadly used mechanism for computing information.[13,16–20] Finally, astrocytes appear to directly release neurotransmitters and other effector molecules ("gliotransmission")[15,21,22] and, at least *in vitro*, have been shown to secrete sleep-promoting substances.[23] Thus, astrocytes could potentially sense sleep-need-generating signals, perform relevant computations, and release signaling molecules to act on a downstream integrator circuit.

The morphology and functions of astrocytes are largely conserved in many animal species, including in the fruit fly *Drosophila melanogaster*.[24] In addition, sleep in *Drosophila* shares all defining behavioral criteria of sleep with mammals.[25–28] Here, we use the fly model to characterize the role of astrocytes in sleep homeostasis and to delineate the mechanisms by which astroglial Ca^{2+} signals encode and transmit

sleep need. Using *ex vivo* and *in vivo* imaging, we show that astrocytic Ca^{2+} levels vary with sleep need and demonstrate a critical role for this Ca^{2+} signaling in sleep homeostasis. Importantly, using a forward genetic approach, we identify tyramine receptor II (TyrRII), a monoaminergic receptor that is transcriptionally upregulated in astrocytes following sleep deprivation and which functions in a Ca^{2+} signaling positive feedback loop to regulate sleep homeostasis. Our data further suggest that this astroglial Ca^{2+} signaling culminates in the upregulation of the secreted molecule Spätzle (Spz), the fly analog of mammalian interleukin-1 (IL-1); Spz then signals to a previously defined sleep drive circuit to control homeostatic rebound sleep. Together, these data support a model wherein astrocytes act as "sensors" of sleep need and encode sleep pressure under conditions of substantial sleep loss. Moreover, the underlying transcriptional and positive-feedback signaling processes provide a mechanistic framework for conceptualizing the delay between and transformation of sleep need to sleep drive.

RESULTS

Ca^{2+} Signaling in Astrocytes Correlates with Sleep Need and Is Necessary for Sleep Homeostasis

On balance, wakefulness is associated with greater neuronal activity.[3,6,29–33] Because astrocytes sense and respond to increases in neuronal activity through Ca^{2+} signaling mechanisms,[10,12,15,18,22,34,35] we first asked whether Ca^{2+} levels in astrocytes vary according to sleep need. To do this, we expressed the genetically encoded Ca^{2+} indicator CaMPARI2[36] in astrocytes and examined *ex vivo* CaMPARI signal in two different neuropil regions (superior medial protocerebrum [SMP] and antennal lobe [AL]) at ZT0–3 (zeitgeber time 0–3), ZT12–15 (mild increase in sleep need), and ZT0–3 following 12 h sleep deprivation (SD) (strong increase in sleep need). Astrocytes exhibit distinct pools of intracellular Ca^{2+} (e.g., soma versus processes) that have different temporal kinetics and may participate in different signaling pathways.[17,18,20,35] Thus, we analyzed CaMPARI signals in both of these locations. As shown in Figures 1A, 1B, and 1D, Ca^{2+} levels in the processes of astrocytes were elevated at ZT12–15, compared to ZT0–3, and further increased at ZT0–3 following SD. In the cell bodies, astrocytic Ca^{2+} levels were not elevated at ZT12–15 but were markedly elevated at ZT0–3 following SD (Figures 1A, 1C, and 1E). To address whether the increases in astrocyte Ca^{2+} concentrations simply reflected a stress response to mechanical SD, we also examined CaMPARI signal at ZT12–15 following 12 h of SD during the daytime. CaMPARI signals were not elevated under these conditions, compared to control flies at ZT12–15 (Figures 1B–1E).

We next examined whether changes in astrocytic Ca^{2+} following SD could be observed in living flies. We performed *in vivo* imaging of Ca^{2+} signals in astrocytic processes in the SMP region using myristoylated GCaMP (myr-GCaMP6s). The frequency of Ca^{2+} transients in the astrocytic processes was significantly increased following SD (Figures 1F–1H, S1A, and S1B), whereas the event size and peak intensity of these Ca^{2+} transients were similar between these two conditions (Figures S1C and S1D). Taken together, our *ex vivo* and *in vivo* data argue that astrocytic Ca^{2+} signaling increases with greater sleep need.

To address whether astrocytic Ca^{2+} signaling is required for the homeostatic regulation of sleep, we sought to identify a molecule that fluxes Ca^{2+} and is important for this process. We conducted a candidate RNAi mini-screen of Ca^{2+}-related channels, transporters, and exchangers and assayed for changes in sleep homeostasis (Figure 2A). Knockdown of an L-type Ca^{2+} channel subunit (Ca-α1D) selectively in astrocytes led to a pronounced reduction in sleep rebound following SD. These findings were next confirmed after backcrossing and with an additional RNAi line targeting Ca-α1D. Knockdown of Ca-α1D in astrocytes substantially reduced sleep recovery following SD (Figures 2B, 2C, and S2A) and did not lead to significant changes in baseline daily sleep time (Figure 2D) or sleep consolidation (Figures S2D and S2E), with mild but inconsistent effects on daytime and nighttime sleep (Figures S2B and S2C). To address the functional role of Ca-α1D in regulating astrocytic Ca^{2+} levels, we measured CaMPARI signal in astrocytes in the AL following SD. As shown in Figures 2E–2G, knockdown of Ca-α1D suppressed the increased Ca^{2+} observed in astrocyte processes and cell bodies following SD. These data suggest that increases in astroglial cytosolic Ca^{2+} are required for normal homeostatic sleep rebound.

Astroglial Ca^{2+} Signaling Triggers Both Acute and Delayed Increases in Sleep Behavior

To examine the consequences of increasing Ca^{2+} levels within astrocytes on sleep behavior, we expressed the temperature-sensitive cation channel dTrpA1 in astrocytes. Interestingly, we found that elevating Ca^{2+} in astrocytes (*alrm-GAL4*) during the night led to two phenotypes: a rapid increase in nighttime sleep during the heat pulse and a persistent increase in daytime sleep following the cessation of the heat pulse (Figures 3A–3C). These two phenotypes were also observed using an additional astrocyte driver (*R86E01-GAL4*) and were reminiscent of the phenotypes seen with activation of the R5 (previously termed R2) ellipsoid body (EB) sleep drive circuit (*R58H05-AD;R46C03-DBD*; Figures 3A–3F).[37] We manually scored fly behavior using video to demonstrate that flies were truly inactive (and not grooming or feeding) during and after thermogenetic activation. These data demonstrated that immobility was specifically increased by these manipulations (Figure S3A). To further confirm that the immobility measured reflects sleep and not simply immobility or paralysis, we assessed arousal threshold. Both during and after thermogenetic activation of astrocytes, flies demonstrated an increased arousal threshold to mild and moderate stimuli but were fully responsive to strong stimuli (Figure S3B). We next asked whether this persistent "sleep rebound" could be induced by a shorter period of astrocyte activation. Indeed, 1 h heat activation of dTrpA1 in astrocytes also triggered a persistent increase in sleep (Figures S3C–S3E). These data suggest that activation of astrocytes is sufficient for inducing sleep behavior and generating homeostatic sleep drive. Moreover, the similarity of the sleep phenotypes seen with activation of astrocytes and R5 neurons suggests that they may act in the same pathway.

TyrRII Is Required for Astroglial Control of Sleep Homeostasis

Little is known about the molecular pathways by which astrocytes regulate sleep. The use of forward genetic screens to

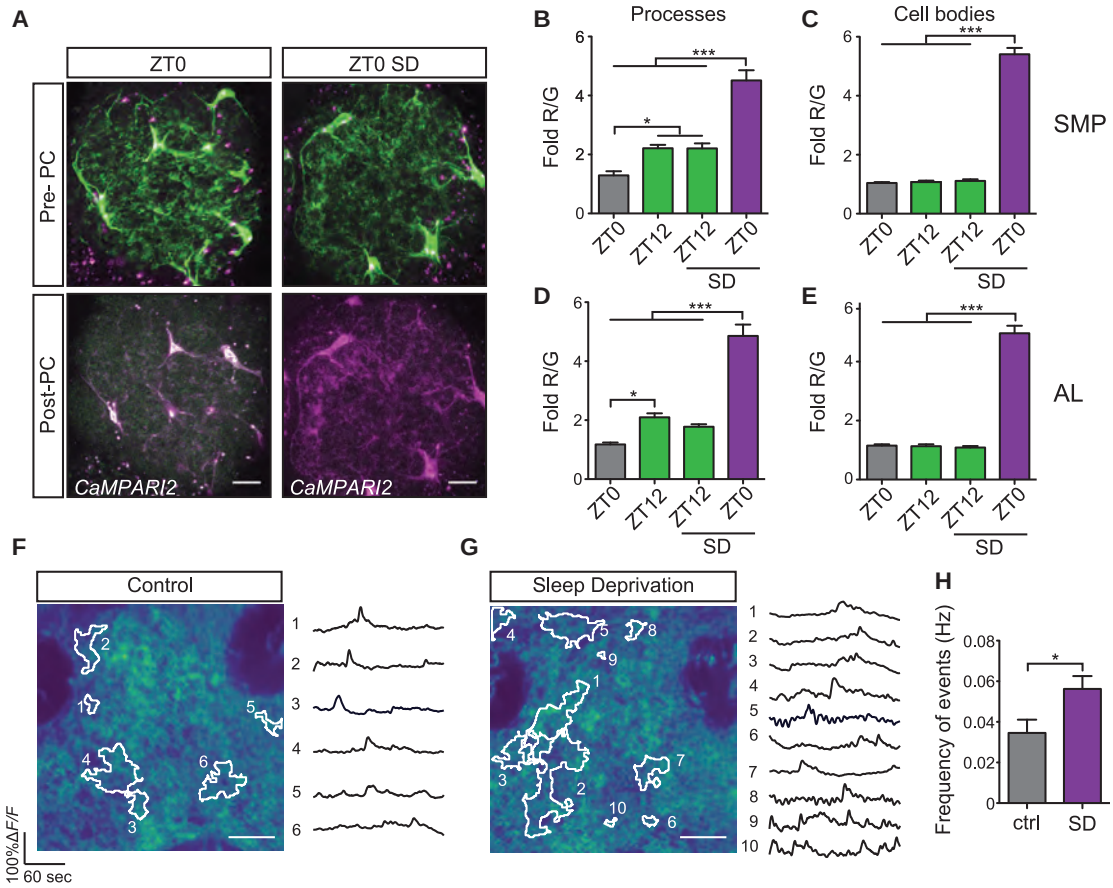

Figure 1. Ca^{2+} Signaling in Astrocytes Correlates with Sleep Need

(A) Representative confocal images of pre-photoconversion (pre-PC) and post-photoconversion (post-PC) CaMPARI2 signal in the antennal lobe (AL) at ZT0 in the presence or absence of sleep deprivation (SD) from *R86E01-GAL4>UAS-CaMPARI2-L398T* flies.

(B–E) CaMPARI2 signal (fold R/G) from astrocyte processes (B and D) or cell bodies (C and E) from superior medial protocerebrum (SMP) or AL from *R86E01-GAL4>UAS-CaMPARI2-L398T* flies at ZT0–3 or ZT12–15 under baseline conditions (AL: n = 5 for ZT0–3 and n = 6 for ZT12–15; SMP: n = 5 for ZT0–3 and n = 6 for ZT12–15) or after 12 h of SD (AL: n = 6 for ZT0–3 and ZT12–15; SMP: n = 6 for ZT0–3 and ZT12–15).

(F and G) Representative 2-photon images (left) and event traces (right) of SMP from non-sleep-deprived control (F) and sleep-deprived (G) *R86E01-GAL4>UAS-myr-GCaMP6s* flies at ZT0–2. Each image is the mean intensity of an entire recording from *in vivo* 2-photon Ca^{2+}-imaging experiments. Data-driven regions of interest (ROIs) that were used to extract event traces are highlighted in white. Corresponding traces and ROIs are numbered.

(H) Frequency of events for control (gray) and sleep-deprived (magenta) flies (n = 9 flies for control and n = 7 flies for SD) expressing membrane-bound GCaMP6s in astrocytes.

Scale bars denote 10 μm in all images. For all bar graphs throughout manuscript, mean ± SEM is shown. In this and subsequent figures, *p < 0.05, **p < 0.01, and ***p < 0.001; ns, not significant. See also Figure S1.

identify novel genes critical for sleep homeostasis has been hindered by the difficulty of performing sleep deprivation robustly and reproducibly on a large scale. To circumvent this problem and identify astrocytic genes required for sleep homeostasis, we capitalized on our finding of persistent sleep drive following astrocyte activation and performed a screen for genes required for this phenotype. From a screen of ~3,200 RNAi lines, we identified ~40 lines that reproducibly suppressed this sleep phenotype (Figure 4A; Table S1). Interestingly, we found that knockdown of the largely uncharacterized receptor TyrRII markedly suppressed the persistent sleep phenotype seen with activation of astrocytes (Figures S4A and S4B). To address whether TyrRII expression in astrocytes is directly required for the homeostatic regulation of sleep, we assessed sleep recovery following 12 h of mechanical SD. Sleep recovery, but not baseline daily sleep, was significantly reduced when TyrRII was knocked down in astrocytes, compared to controls (Figures 4B–4D and S4C). In contrast, knockdown of TyrRII in astrocytes did not yield significant effects on baseline daytime sleep, nighttime sleep, or sleep consolidation (Figures S4D–S4G).

TyrRII Is Upregulated with Sleep Loss and Participates in a Positive-Feedback, Ca^{2+}-Signaling Mechanism

TyrRII has previously been shown to be broadly responsive to a variety of monoamines and, given that monoamine release is generally associated with arousal,[38–41] this system could represent an elegant mechanism for astrocytes to track wakefulness and consequently homeostatic sleep need. Because monoaminergic receptor expression is often tightly regulated by diverse signaling mechanisms,[42] we examined whether *tyrRII*

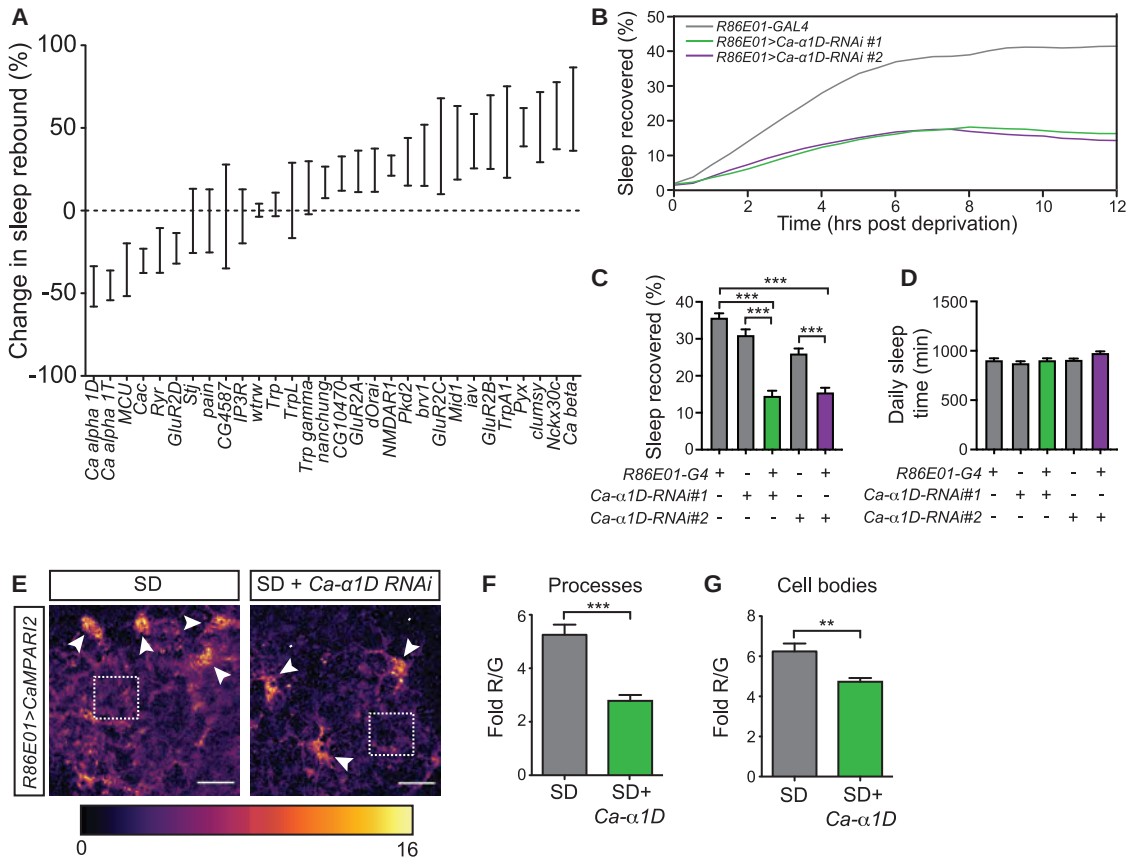

Figure 2. Ca^{2+} Signaling in Astrocytes Is Required for Sleep Homeostasis

(A) Mechanical deprivation mini-screen of astrocyte Ca^{2+}-related channels, transporters, and exchangers. Relative change in sleep rebound for *R86E01-GAL4>UAS-RNAi* flies expressed as a percentage of sleep rebound observed in *R86E01-GAL4>UAS-empty vector* flies is shown.

(B) Sleep recovery curves for *R86E01-GAL4* > *iso31* (gray) versus *R86E01-GAL4* > *UAS-Ca-α1D-RNAi#1* (green) and *R86E01-GAL4* > *UAS-Ca-α1D-RNAi#2* (magenta) flies.

(C and D) Sleep recovered (%; C) and daily sleep amount (D) for *R86E01-GAL4* > *iso31* (n = 54), *iso31* > *UAS-Ca-α1D-RNAi#1* (n = 46), *R86E01-GAL4* > *UAS-Ca-α1D-RNAi#1* (n = 46), *iso*31 > *UAS-Ca-α1D-RNAi#2* (n = 63), and *R86E01-GAL4* > *UAS-Ca-α1D-RNAi#2* (n = 50) flies. For (B)–(D), N = 3 independent trials, with similar results obtained for each trial.

(E) Pixel-by-pixel heatmap of CaMPARI2 photoconversion signal in the AL region at ZT0–3 following 12 h SD in *R86E01-GAL4>UAS-CaMPARI2-L398T* flies, in the presence or absence of *UAS-Ca-α1D-RNAi#1.* Dotted squares highlight Ca^{2+} signals from fine astrocyte processes, and white arrows denote cell bodies. Scale bars denote 10 μm.

(F and G) Quantification of average CaMPARI2 signal (fold R/G) from ROIs targeting astrocyte processes (F) or cell bodies (G) represented in (E).

See also Figure S2.

expression varied according to sleep need. We assessed astrocyte expression of *tyrRII* mRNA using TRAP-qPCR (translating ribosome affinity purification followed by quantitative PCR).[43] To do this, we expressed RpL10a::EGFP in astrocytes and immunopurified actively translating mRNA using magnetic beads coated with anti-GFP antibodies (Figure 4E). As expected, immunoprecipitates were dramatically enriched for a glial marker (*repo*), compared to a neuronal marker (*nSyb*; Figure 4F). Interestingly, *tyrRII* mRNA was markedly elevated ~10-fold after sleep deprivation (Figure 4G). This increase could be recapitulated by dTrpA1 activation of astrocytes, suggesting that the increase in *tyrRII* following sleep deprivation is Ca^{2+} dependent (Figures 4H, 4I, S4H, and S4I).

We next asked whether TyrRII protein levels were also increased following sleep deprivation. To address this question, we used a MiMIC transposon insertion,[44] where GFP is fused in frame into the 2nd extracellular loop of the TyrRII protein. Consistent with our findings with *tyrRII* mRNA, TyrRII::GFP expression was substantially increased following 12 h SD versus non-SD controls, both in terms of number and size of puncta (Figures S4J–S4L). Interestingly, super-resolution microscopy revealed that the sleep-deprivation-mediated increase in TyrRII::GFP expression within the AL neuropil was largely localized to bulbous structures within astrocytic processes (Figure S4M). These structures were also observed by *R86E01-GAL4*-driven tdTomato expression independent of sleep need state, suggesting that they are not a direct consequence of either sleep deprivation or the expression of TyrRII::GFP.

Our TRAP-qPCR data suggested that the upregulation of *tyrRII* mRNA following SD is dependent on astrocytic intracellular Ca^{2+} (Figure 4I). To directly test whether astrocytic Ca^{2+} signaling is required for the sleep-need-induced elevation in

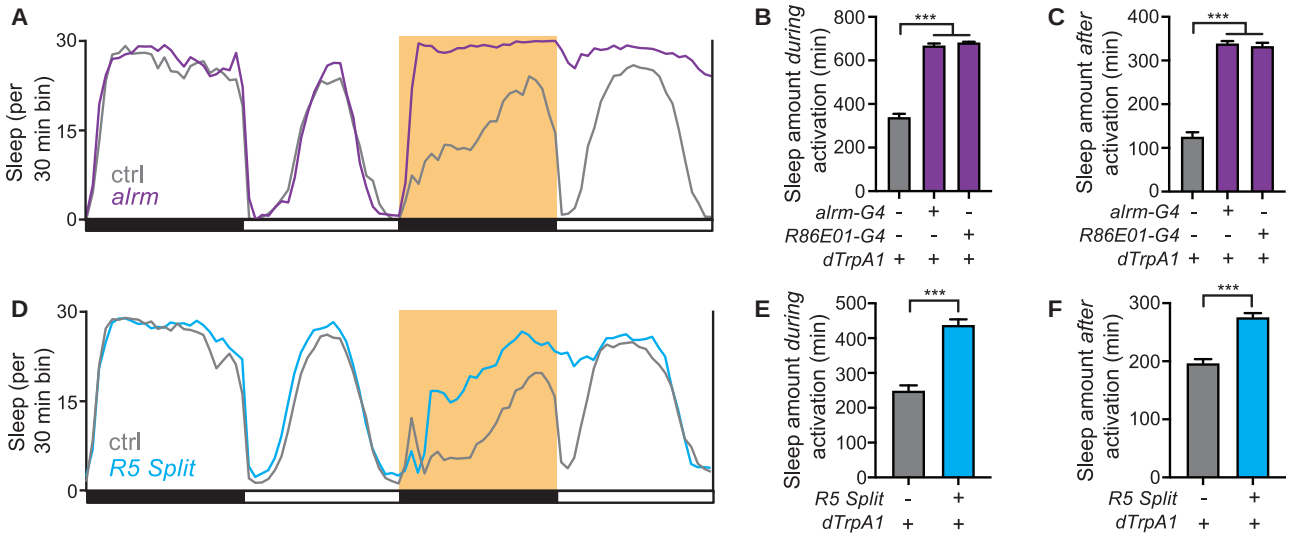

Figure 3. Astrocyte Activation Induces Both Proximate and Delayed Sleep

(A) Sleep profile for *iso31* > *UAS-dTrpA1* (gray) versus *alrm-GAL4>UAS-dTrpA1* flies (magenta). Highlighted period denotes 12 h dTrpA1 activation at 28°C.

(B and C) Sleep amount over a 12-h period during (B) or 6 h after (C) dTrpA1 activation for *iso31* > *UAS-dTrpA1* (n = 81), *alrm-GAL4>UAS-dTrpA1* (n = 40), and *R86E01-GAL4>UAS-dTrpA1* flies (n = 29). For the number of independent trials, N = 3, 3, and 2 for *iso31* > *UAS-dTrpA1*, *alrm-GAL4>UAS-dTrpA1*, and *R86E01-GAL4>UAS-dTrpA1*, respectively. Similar results were obtained in each trial.

(D) Sleep profile for *iso31* > *UAS-dTrpA1* (gray) versus *R58H05-AD;R46C03-DBD* > *UAS-dTrpA1* (cyan). Highlighted period denotes 12 h dTrpA1 activation at 29°C.

(E and F) Sleep amount over a 12-h period during (B) or 6 h after (C) dTrpA1 activation for *iso31* > *UAS-dTrpA1* (n = 94) and *R58H05-AD;R46C03-DBD* > *UAS-dTrpA1* (n = 79) flies. For (D)–(F), N = 3 independent trials, with similar results obtained for each trial.

See also Figure S3.

TyrRII::GFP, we performed RNAi knockdown of Ca-α1D in astrocytes and quantified TyrRII::GFP expression before and after SD. As shown in Figures 5A–5C, TyrRII::GFP expression following SD, but not under baseline conditions, was significantly reduced with concomitant knockdown of Ca-α1D, compared to controls. Prior studies have shown that monoaminergic signaling induces Ca^{2+} elevations in astrocytes in both flies and mice.[45,46] Thus, TyrRII might produce an amplifying positive-feedback loop in astrocytes—not only does TyrRII expression depend on intracellular Ca^{2+} levels, but the higher levels of TyrRII expression following SD contribute to further increases in Ca^{2+} levels. To address this possibility, we examined whether loss of TyrRII suppressed the elevation of intracellular Ca^{2+} seen in astrocytes after prolonged wakefulness. Following SD, CaMPARI signal in both astrocyte processes and cell bodies was substantially reduced in *R86E01-GAL4>UAS-TyrRII-RNAi* animals, compared to controls (Figures 5D–5F). Taken together, these data suggest that, as sleep need accrues during protracted arousal, TyrRII amplifies Ca^{2+} signaling in a positive-feedback loop, priming astrocytes and sensitizing them to monoamines.

Activating Astrocytes Inhibits an Arousal Circuit

Not only are the underlying molecular pathways unclear, but the circuit mechanisms by which astrocytes signal sleep need are also unknown. We first asked how astroglial activation would impact an arousal circuit. To address this question, we performed patch-clamp recordings of the large ventrolateral clock neurons (l-LNvs). As clock neurons that modulate arousal,[47–49] the firing rate of the l-LNvs is under circadian control,[50–52] but their sensitivity to sleep need is unknown. Therefore, we first examined whether l-LNv firing is altered following 12 h of SD; indeed, their firing rate at ZT0–2 was significantly reduced and their resting membrane potential was hyperpolarized after SD (Figures S5A–S5C). We then assessed the impact of dTrpA1 activation of astrocytes on l-LNv activity. *alrm>dTrpA1*-mediated astrocyte activation led to a significant reduction in spiking frequency and resting membrane potential, whereas heat treatment alone (*UAS-dTrpA1*) had no effect on either (Figures S5D–S5H). Similar observations were made using *R86E01-GAL4* (Figures S5I and S5J). These data suggest that the increased sleep induced by astroglial activation may result, at least in part, from acute inhibition of arousal-promoting circuits.

Astrocyte-Derived Spätzle Transmits Sleep Need to the R5 Sleep Drive Circuit via the Toll Receptor

We next asked whether astrocytes signal sleep need to a sleep-promoting circuit. The similarity of the sleep phenotypes seen with activation of astrocytes and the R5 sleep drive circuit (Figure 3) led us to hypothesize that astrocytes act upstream of the R5 neurons. We previously demonstrated that intracellular Ca^{2+} levels in R5 are elevated with greater sleep need and that this higher intracellular Ca^{2+} was critical for the synaptic plastic changes encoding sleep drive in these neurons.[37] Thus, we assessed whether thermogenetic activation of astrocytes would lead to a similar increase in R5 intracellular Ca^{2+}. To do this, we first generated a QF2 driver line that labeled R5 EB ring neurons (*R58H05-QF2*; Figures S6A and S6B). Importantly, we found that overnight dTrpA1 activation of astrocytes led to a

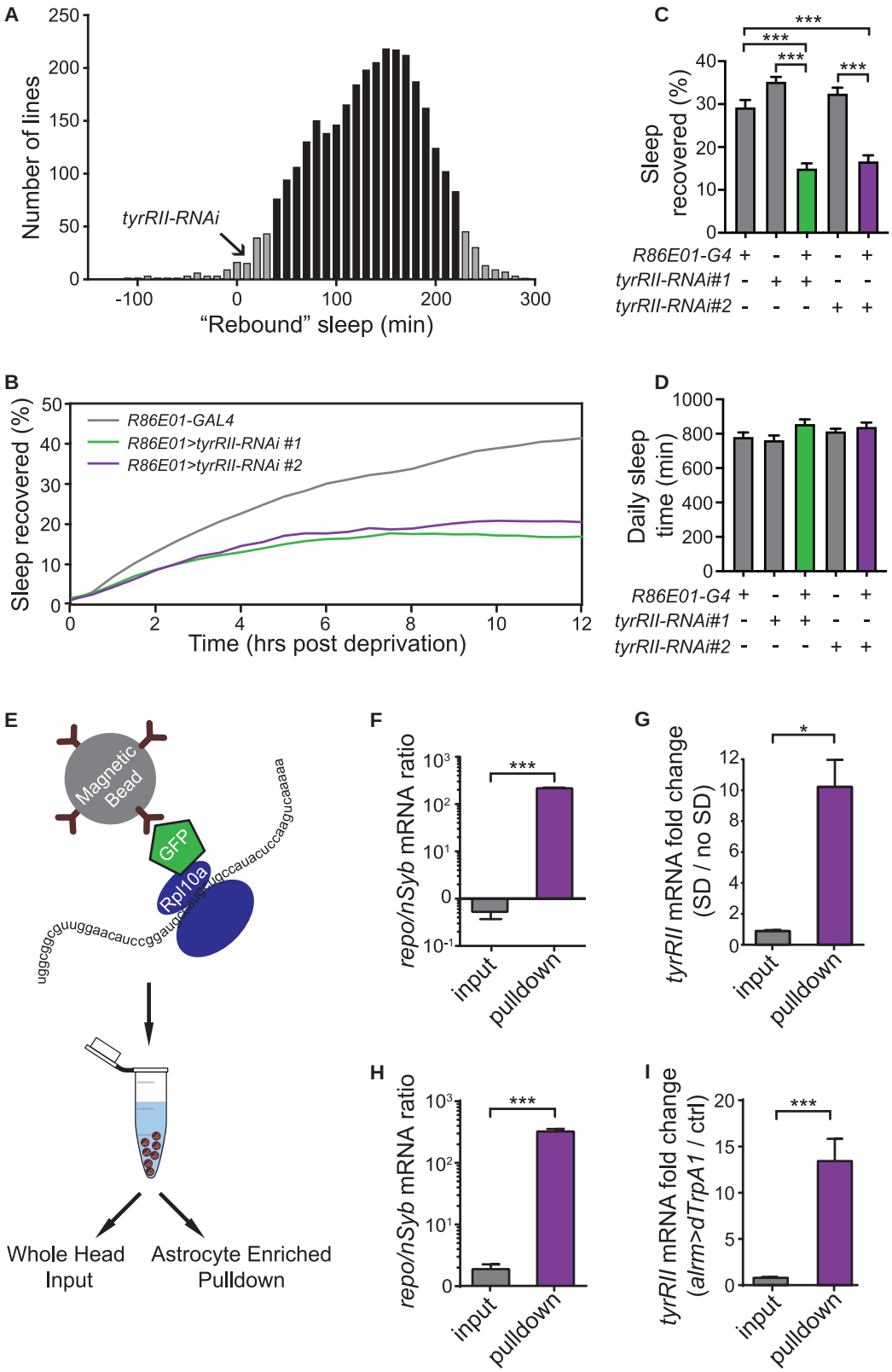

(legend on next page)

substantial elevation of GCaMP signal in the R5 neurons the next morning (Figures 6A and 6B).

What is the molecular mechanism by which astrocytes signal to the R5 neurons? In the course of testing putative astroglial signaling molecules on sleep behavior, we found *spätzle* (*spz*), the *Drosophila* analog of IL-1. Because IL-1 has previously been implicated in the homeostatic regulation of sleep in mammals,[53] we focused on this gene. To address whether *spz* expression was altered in response to changes in sleep need, we performed TRAP-qPCR and found that *spz* mRNA was increased ~9-fold in astrocytes following SD or thermogenetic activation (Figures 6C and 6D), supportive of a role for astrocytic Spz in relaying sleep need. Knockdown of *spz* in astrocytes significantly reduced sleep recovery following SD (Figures 6E, 6F, and S6C). Under baseline conditions, knockdown of astroglial *spz* led to a mild increase in daily sleep time and daytime sleep, with no consistent effects on nighttime sleep and sleep consolidation (Figures 6G and S6D–S6G). These data suggest that astrocytes signal to the R5 sleep drive neurons to promote sleep and that Spz is a candidate signaling molecule in this process.

Toll is a well-characterized receptor for Spz,[54,55] and interestingly, recent data suggest that Toll is enriched within the EB in the adult brain.[56] Thus, we hypothesized that astrocyte-derived Spz signals to Toll receptors on R5 neurons to signal sleep need. To test this hypothesis, we first examined the effects of Toll knockdown on intracellular Ca^{2+} levels in R5 neurons. As shown in Figures 7A and 7B, knockdown of Toll in R5 neurons largely suppressed the sleep-deprivation-induced increase in intracellular Ca^{2+} levels in these cells. Next, we assessed the effects of Toll knockdown in R5 neurons on sleep behavior. Flies expressing *UAS-Toll-RNAi* or *UAS-Toll-miR* transgenes in the R5 neurons exhibited a significant reduction in sleep recovery following SD (Figures 7C, 7D, and S7A) but no significant alterations in daily sleep time, daytime sleep, nighttime sleep, and sleep consolidation under baseline conditions (Figures 7E and S7B–S7E).

To investigate a functional role for R5 neurons downstream of astrocyte signaling, we performed behavioral epistasis experiments. We thermogenetically activated astrocytes while simultaneously silencing the R5 neurons and found that the increase in sleep during activation was significantly reduced, and the induced "rebound" sleep was essentially abolished (Figures 7F–7H). We previously showed that the R5 neurons act indirectly upstream of the sleep-promoting ExFl2 neurons,[37] and so we also addressed whether similar data would be obtained with manipulation of the ExFl2 neurons. As shown in Figures 7F–7H, silencing ExFl2 neurons led to a marked decrease in sleep during astroglial activation and a significant reduction in induced rebound sleep. Taken together, these findings suggest that astrocytes signal sleep need by upregulating and releasing Spz, which activates R5 neurons via Toll receptors to promote sleep drive.

DISCUSSION

Although astrocytes have been implicated in the homeostatic regulation of sleep,[8] their specific role and the underlying mechanisms are unresolved. Our data support a role for astrocytes as sensors of sleep need and define signaling mechanisms within these cells that mediate the integration and transmission of this information to a downstream homeostatic sleep circuit (Figure 7I). In this model, neural activity is sensed by astrocytic processes, leading to an increase in Ca^{2+} levels, which depends at least in part on specific L-type voltage-gated Ca^{2+} channels (VGCC).[57–60] Although astrocytes have been shown to exhibit hyperpolarized membrane potentials with small depolarizations,[57,61] this particular subtype of L-type VGCC can be activated at substantially lower membrane potentials than other members of this channel family.[62] Interestingly, two recent studies in mice found that intracellular Ca^{2+} levels in astrocytes vary across sleep/wake states and that Ca^{2+} signaling in these cells is required for normal sleep architecture and responses to sleep deprivation.[63,64] These observations suggest a conserved role for astroglial Ca^{2+} signaling in sleep homeostasis.

Our model further suggests that, as the increased neural activity persists, Ca^{2+}-mediated transcription of TyrRII is induced in astrocytes. TyrRII is relatively unstudied, but *in vitro* data suggest

Figure 4. *tyrRII* Is Upregulated with Sleep Need and Required in Astrocytes for Homeostatic Sleep Rebound

(A) Histogram for RNAi genetic screen for *alrm-GAL4 > UAS-dTrpA1, UAS-RNAi* flies (n = 3,207 genes; n = 4 flies per genotype) showing "rebound" sleep (6 h post-activation) induced by 1 h of heat (31°C) from ZT0–1, as described in the STAR Methods. The amount of rebound sleep for *alrm-GAL4 > UAS-TyrRII-RNAi#1*-expressing flies is noted. Bars in gray denote values lying ± 2.5 SD from the mean.

(B) Sleep recovery curves for *R86E01-GAL4 > iso31* (gray) versus *R86E01-GAL4 > UAS-TyrRII-RNAi#1* (green) and *R86E01-GAL4 > UAS-TyrRII-RNAi#2* (magenta) flies after overnight (12 h) SD.

(C and D) Sleep recovered (%; C) and daily sleep amount (D) for *R86E01-GAL4 > iso31* (n = 51), *iso31 > UAS-TyrRII-RNAi#1* (n = 40), *R86E01-GAL4 > UAS-TyrRII-RNAi#1* (n = 43), *iso31 > UAS-TyrRII-RNAi#2* (n = 46), and *R86E01-GAL4 > UAS-TyrRII-RNAi#2* (n = 46). For the number of independent trials, N = 3, 3, 3, 4, and 4 for *R86E01-GAL4 > iso31*, *iso31 > UAS-TyrRII-RNAi#1*, *R86E01-GAL4 > UAS-TyrRII-RNAi#1*, *iso31 > UAS-TyrRII-RNAi#2*, and *R86E01-GAL4>UAS-TyrRII-RNAi#2*, respectively. Similar results were obtained in each trial.

(E) Schematic of translating ribosomal affinity purification (TRAP) procedure for isolating actively translating mRNA from genetically defined astrocytes in whole fly heads.

(F) Relative ratio of astrocyte marker (*repo*) and neural marker (*nSyb*) mRNA level in whole-head flowthrough (input, n = 3 replicates) versus astrocyte-TRAP (pull-down; n = 3 replicates) samples from sleep deprivation experiment.

(G) Relative change in *tyrRII* mRNA level in astrocyte-TRAP (pull-down) versus whole head (input) samples from *R86E01-GAL4 > UAS-Rpl10a::EGFP* flies that were sleep deprived (SD) (n = 3 replicates) versus non-SD (no SD) (n = 3 replicates).

(H) Relative ratio of astrocyte marker (*repo*) and neural marker (*nSyb*) mRNA level in whole-head flowthrough (input; n = 3 replicates) versus astrocyte-TRAP (pull-down; n = 3 replicates) samples from experiments where astrocytes are thermogenetically activated.

(I) Relative fold change in *tyrRII* mRNA level in astrocyte-TRAP (pull-down) versus whole head (input) samples from thermogenetically activated *alrm-QF2 > QUAS-dTrpA1; R86E01-GAL4 > UAS-Rpl10a::EGFP* (n = 3 replicates) versus *iso31 > QUAS-dTrpA1; R86E01-GAL4 > UAS-Rpl1a::EGFP* ("ctrl"; n = 3 replicates) flies.

See also Figure S4 and Table S1.

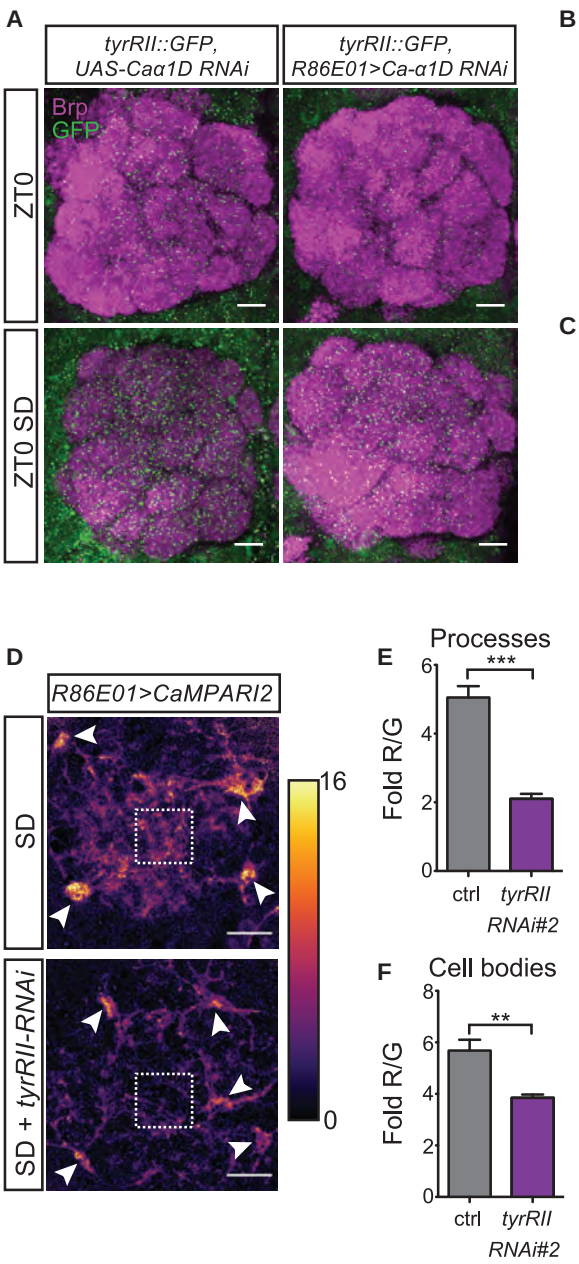

Figure 5. Astrocytic TyrRII Is Upregulated with Sleep Need and Participates in a Positive-Feedback Calcium-Signaling Mechanism

(A) Representative images of TyrRII::GFP signal at the AL in the presence or absence of 12 h sleep deprivation from *iso31* > *UAS-Ca-α1D RNAi#1, Mi{PT-GFSTF.2}TyrRII*^{MI12699}/+ or *R86E01-GAL4* > *UAS-Ca-α1D RNAi#1, Mi{PT-GFSTF.2}TyrRII*^{MI12699}/+ flies. Whole-mount brains were collected from ZT0 to ZT1 and immunostained with anti-GFP (green) and anti-BRP (magenta).

(B and C) Number (B) and size (C) of TyrRII::GFP puncta in the AL under baseline (ZT0) or SD conditions with (magenta) or without (gray) *Ca-α1D* knockdown (n = 8 for all groups and conditions).

(D) Pixel-by-pixel heatmap of CaMPARI2 photoconversion signal in the AL region from ZT0 to ZT3 following 12 h SD in *R86E01-GAL4>UAS-CaMPARI2-L398T* flies in the presence (n = 9) and absence (n = 10) of *UAS-TyrRII-RNAi#2*. Dotted squares highlight Ca^{2+} signals from fine astrocyte processes, and white arrows denote cell bodies.

(E and F) Quantification of CaMPARI2 signal (fold R/G) from astrocyte processes (E) or cell bodies (F).

Scale bars denote 20 μm in (A) and 10 μm in (D). See also Figure S4.

that it responds non-specifically to multiple monoamines.[65] Thus, its upregulation in astrocytes should sensitize these cells to signaling via monoamines, which are intimately associated with wakefulness.[66] The requirement for monoamines in this pathway may provide a logic gate for the system, imparting specificity to the signaling mechanism acting downstream of neural activity, whose semantic properties may be too broad. TyrRII itself is required for further Ca^{2+} elevations, forming a positive-feedback loop.

Our data suggest that this amplification of astrocytic Ca^{2+} signals results in transcriptional upregulation of *spz*, the fly analog of IL-1. There is an accumulating body of evidence implicating IL-1 in sleep homeostasis in mammals,[53,67–69] and our findings demonstrating a functional role for astrocytic Spz in sleep homeostasis demonstrate that these mechanisms are conserved from invertebrates to vertebrates. In our model, Spz is released from astrocytes under conditions of strong sleep need and transmits this information by signaling to a central sleep drive circuit (the R5 neurons) to promote homeostatic sleep rebound. It is worth noting that fly astrocytes likely possess multiple output mechanisms to regulate sleep, as they not only activate sleep-promoting neurons (R5 neurons) but also inhibit arousal-promoting neurons (l-LNvs).

From a broader perspective, our model draws attention to a fundamental, yet poorly understood, aspect of sleep homeostasis—how a highly dynamic input (i.e., neural activity operating on the millisecond timescale) is integrated and transformed to generate a sleep homeostatic force that functions on a significantly slower timescale. Although the precise identity of the signals embodying sleep need remain unclear, there is substantial experimental and conceptual support for the notion that neural activity increases with wakefulness[70] and is a key trigger for this process.[3,30] Yet the dynamic mechanisms by which this neural activity and, by extension, sleep need are transformed to sleep drive are unknown. The homeostatic regulation of processes and behaviors involving bistable states, such as sleep versus wakefulness, requires a prominent delay between the detection of the disturbance and the generation of the response.[71,72] In addition, the stability and switching between such bistable states can be facilitated by positive-

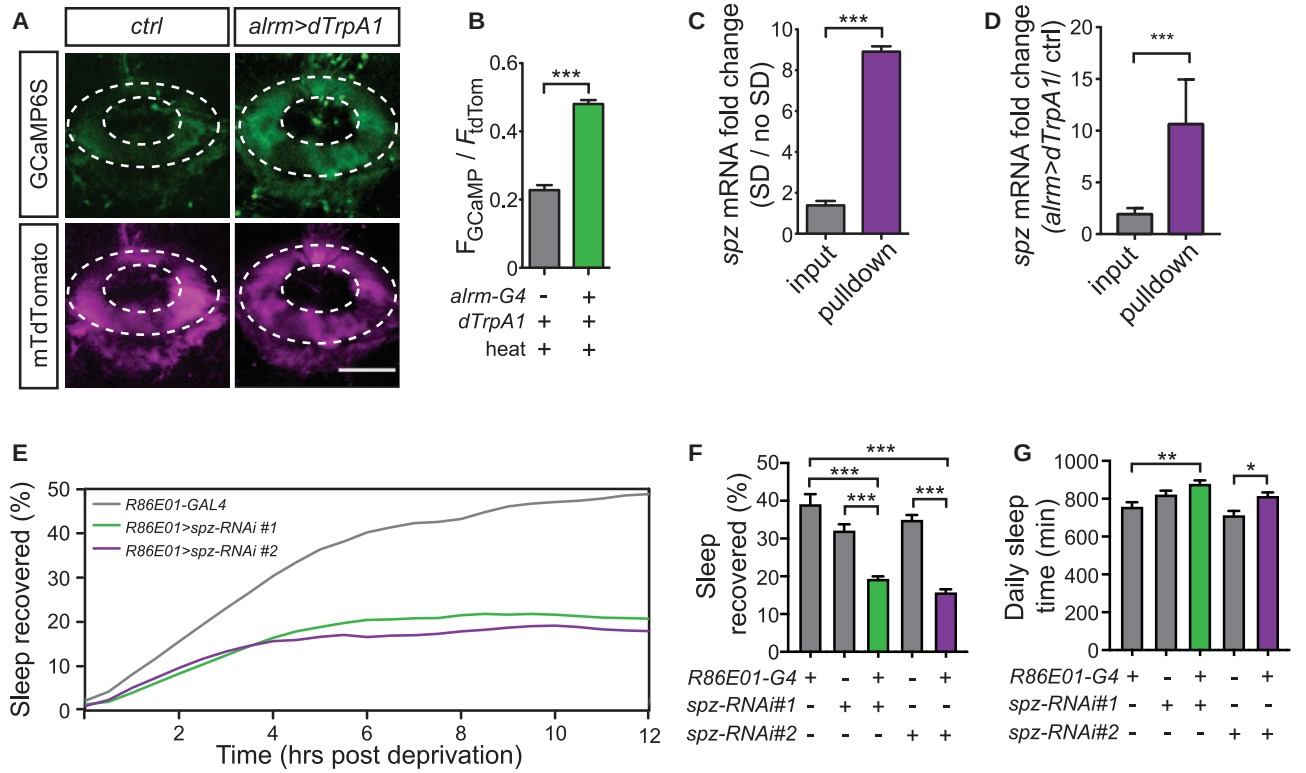

Figure 6. Spätzle, an IL-1 Analog, Is Upregulated in Astrocytes with Sleep Need and Required for Homeostatic Sleep Rebound

(A and B) Representative images of GCaMP (upper panels) and tdTomato (lower panels) fluorescence intensity (A) and relative GCaMP fluorescence intensity (B) in the R5 ring of *iso31* > *UAS-dTrpA1; R58H05-QF2* > *QUAS-GCaMP6s, QUAS-mtdTomato::3XHA* (ctrl; n = 5) versus *alrm-GAL4* > *UAS-dTrpA1; R58H05-QF2* > *QUAS-GCaMP6s, QUAS-mtdTomato::3XHA* (n = 4) flies at ZT3–5 after 12 h of heat treatment from ZT12 to ZT24 at 28°C. For (A), dashed lines indicate the R5 ring and scale bar denotes 20 μm.

(C) Relative change in *spz* mRNA level in SD (n = 3 replicates) versus no SD (n = 3 replicates) flies from astrocyte-TRAP (pull-down) versus whole head (input) samples. Control *repo/nSyb* ratios for this experiment are provided in Figure 4F.

(D) Relative fold change in *spz* mRNA level in thermogenetically activated *alrm-GAL4>UAS-dTrpA1* (n = 3 replicates) versus *iso31* > *UAS-dTrpA1* (n = 3 replicates) flies from astrocyte-TRAP (pull-down) versus whole head (input) samples. Control *repo/nSyb* ratios for this experiment are provided in Figure 4H.

(E) Sleep recovery curve for *R86E01-GAL4* > *iso31* (gray), *R86E01-GAL4* > *UAS-spz-RNAi#1* (green), and *R86E01-GAL4* > *UAS-spz-RNAi#2* (magenta) flies.

(F and G) Sleep recovered (%; F) and daily sleep amount (G) for *R86E01-GAL4* > *iso31* (n = 56), *iso31* > *UAS-spz-RNAi#1* (n = 48), *R86E01-GAL4* > *UAS-spz-RNAi#1* (n = 65), *iso31* > *UAS-spz-RNAi#2* (n = 50), and *R86E01-GAL4* > *UAS-spz-RNAi#2* (n = 85) flies. For the number of independent trials, N = 3, 3, 3, 4, and 4 for *R86E01-GAL4* > *iso31*, *iso31* > *UAS-spz-RNAi#1*, *R86E01-GAL4* > *UAS-spz-RNAi#1*, *iso31* > *UAS-spz-RNAi#2*, and *R86E01-GAL4* > *UAS-spz-RNAi#2*, respectively. Similar results were obtained for each trial.

See also Figures S5 and S6.

feedback loops.[38,73–75] We speculate that the transcription/translation of TyrRII, coupled with the generation of a positive-feedback loop, provide a timing delay followed by a more rapid elevation in astroglial Ca^{2+} after reaching a set threshold, thus enabling a non-linear response to the continual sampling of sleep need. The transcriptional/translation upregulation of Spz could represent an additional layer of delay.

STAR★METHODS

Detailed methods are provided in the online version of this paper and include the following:

- KEY RESOURCES TABLE
- RESOURCE AVAILABILITY
  - Lead Contact
  - Materials Availability
  - Data and Code Availability
- EXPERIMENTAL MODEL AND SUBJECT DETAILS
- METHOD DETAILS
  - Fly Stocks and maintenance
  - Nomenclature
  - Molecular Biology
  - Behavioral Analyses
  - Imaging
  - Electrophysiology
  - Translating ribosomal affinity purification with quantitative polymerase chain reaction
- QUANTIFICATION AND STATISTICAL ANALYSIS

SUPPLEMENTAL INFORMATION

Supplemental Information can be found online at https://doi.org/10.1016/j.cub.2020.10.012.

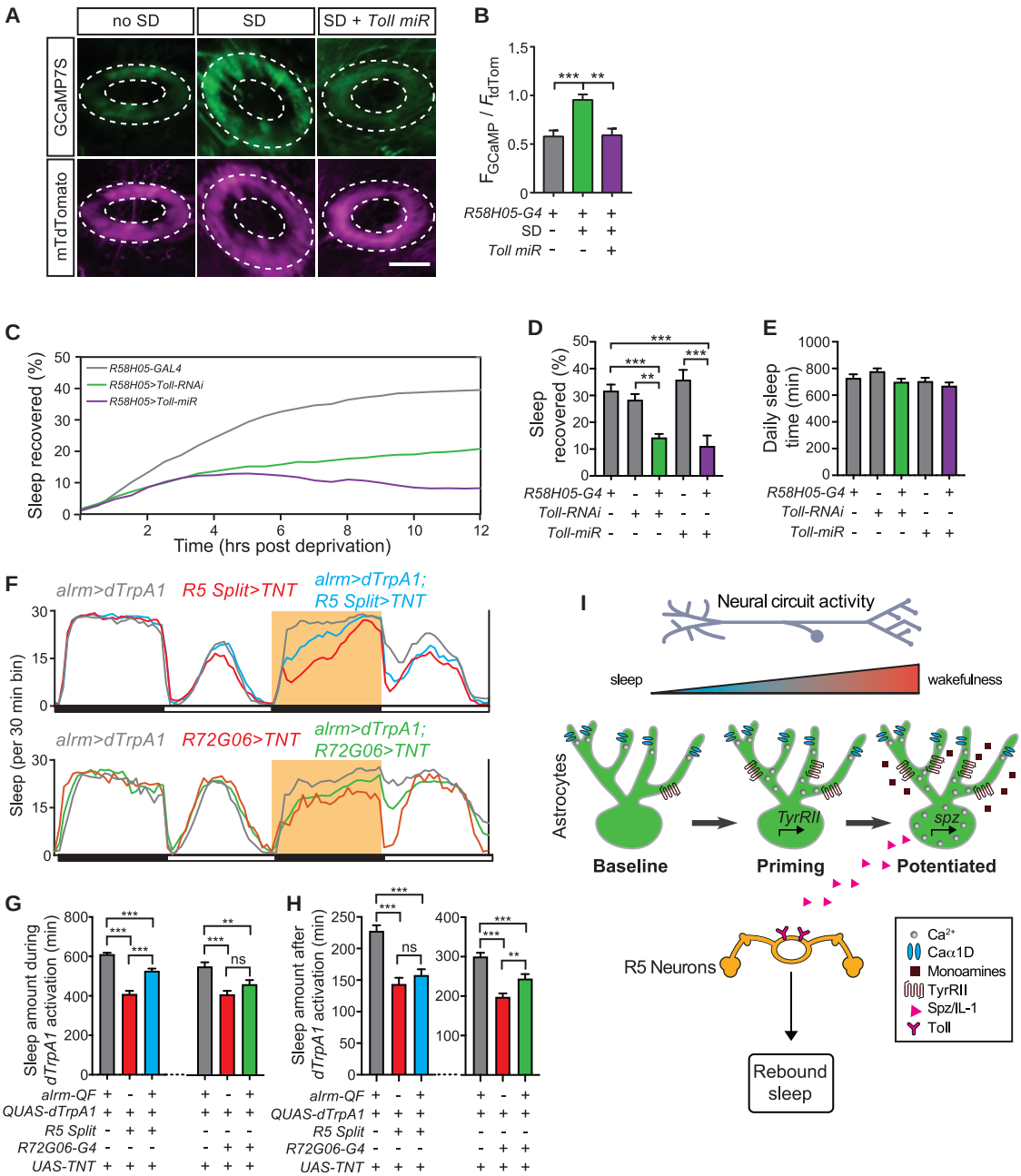

Figure 7. Astrocytes Signal Sleep Need to the R5 Sleep Drive Circuit via the Toll Receptor

(A and B) Representative images of GCaMP (upper panels) and tdTomato (lower panels) fluorescence intensity (A) and relative GCaMP fluorescence intensity (B) in the R5 ring of *R58H05-GAL4 > UAS-GCaMP7s, UAS-CD4::tdTomato* flies from ZT3 to ZT5 in the absence (no SD; n = 8) or presence (SD; n = 8) of 24 h SD versus *R58H05-GAL4 > UAS-GCaMP7s, UAS-CD4::tdTomato, UAS-Toll-miR* (SD + Toll miR; n = 7) following 24 h SD. For (A), dashed lines indicate the R5 ring and scale bar denotes 20 μm.

(C) Sleep recovery curve of *R58H058-GAL4 > iso31* (gray), *R58H05-GAL4 > UAS-Toll-RNAi* (green), and *R58H05-GAL4 > UAS-Toll-miR* (magenta).

(D and E) Sleep recovered (%; D) and daily sleep amount (E) for *R58H05-GAL4 > iso31* (n = 84), *iso*31 > *UAS-Toll-RNAi* (n = 84), *R58H05-GAL4>UAS-Toll-RNAi* (n = 100), *iso*31 > *UAS-Toll-miR* (n = 76), and *R58H05-GAL4>UAS-Toll-miR* (n = 79) flies. For the number of independent trials, N = 4, 3, 3, 3, and 3 for *R58H05-GAL4 > iso31*, *iso31 > UAS-Toll-RNAi*, *R58H05-GAL4>UAS-Toll-RNAi*, *iso31 > UAS-Toll-miR*, and *R58H05-GAL4 > UAS-Toll-miR*, respectively.

(F) Sleep profile for *alrm-QF2 > QUAS-dTrpA1* (2nd); *iso31 > UAS-TNT* (gray), *iso31 > QUAS-dTrpA1* (2nd); *R58H05-AD;R46C03-DBD > UAS-TNT* (red), and *alrm-QF2 > QUAS-dTrpA1* (2nd); *R58H05-AD;R46C03-DBD > UAS-TNT* flies (cyan) is in upper panel. Sleep profile for *alrm-QF2 > QUAS-dTrpA1* (3rd); *iso31 > UAS-TNT* (gray), *iso31 > QUAS-dTrpA1* (3rd); *R72G06-GAL4 > UAS-TNT* (red), and *alrm-QF2 > QUAS-dTrpA1* (3rd); *R72G06-GAL4 > UAS-TNT* flies (green) is in lower panel. Highlighted period denotes 12 h dTrpA1 activation at 28°C.

(G and H) (Left) Sleep amount over a 12-h period during (G) or 6 h after (H) dTrpA1 activation for *alrm-QF2 > QUAS-dTrpA1* (2nd); *iso31 > UAS-TNT* (n = 94), *iso31 > QUAS-dTrpA1* (2nd); *R58H05-AD;R46C03-DBD > UAS-TNT* (n = 88), and *alrm-QF2 > QUAS-dTrpA1* (2nd); *R58H05-AD;R46C03-DBD > UAS-TNT* flies (n = 93).

(legend continued on next page)

ACKNOWLEDGMENTS

We thank M. Freeman, R. Jackson, T. Littleton, C. Potter, G. Rubin, and E. Schreiter for kindly sharing reagents. We thank A.M. Ingiosi and M.G. Frank for sharing unpublished results. We also thank the Bloomington Stock Center (supported by NIH grant P40OD018537), the Vienna *Drosophila* Stock Center (http://stockcenter.vdrc.at/), and the TRiP at Harvard Medical School (supported by NIH grant R01GM084947) for fly stocks used in this study. We thank members of the Wu lab for discussion. This work was supported by NINDS Center Grant P30 NS050274 for use of the Core Machine Shop and the Multiphoton Imaging Core, ERC Starting Grant 758580 (S.L.), and NIH grants K99NS101065 (M.T.), R01NS094571-03S1 (M.N.W.), R01NS100792 (M.N.W.), and R01NS079584 (M.N.W.).

AUTHOR CONTRIBUTIONS

Conceptualization, I.D.B., S. Liu, and M.N.W.; Methodology, I.D.B., M.F.K., E.H., M.T., and M.N.W.; Software, I.D.B. and M.F.K.; Investigation, I.D.B., M.F.K., E.-S.B., E.H., K.P., S. Luu, H.I., M.C.W.H., M.B., and M.T.; Writing – Original Draft, I.D.B. and M.N.W.; Writing – Review & Editing, I.D.B., M.F.K., E.-S.B., E.H., K.P., S. Luu, H.I., M.B., M.C.H., M.T., S. Liu, and M.N.W.; Resources, S. Liu and M.N.W.; Visualization, I.D.B., M.F.K., E.H., and E.-S.B.; Supervision, I.D.B., M.T., S. Liu, and M.N.W.; Funding Acquisition, M.T., S. Liu, and M.N.W.

DECLARATION OF INTERESTS

The authors declare no competing interests.

Received: May 7, 2020
Revised: September 17, 2020
Accepted: October 7, 2020
Published: November 12, 2020

REFERENCES

1. Blanchard, S., and Bronzino, J.D. (2012). Anatomy and physiology. In Introduction to Biomedical Engineering, Third Edition, J.D. Enderle, and J.D. Bronzino, eds. (Academic), pp. 75–132.
2. Reichert, S., Pavón Arocas, O., and Rihel, J. (2019). The neuropeptide galanin Is required for homeostatic rebound sleep following increased neuronal activity. Neuron *104*, 370–384.e5.
3. Cirelli, C., and Tononi, G. (2019). Linking the need to sleep with synaptic function. Science *366*, 189–190.
4. Huber, R., Ghilardi, M.F., Massimini, M., and Tononi, G. (2004). Local sleep and learning. Nature *430*, 78–81.
5. Rector, D.M., Schei, J.L., Van Dongen, H.P., Belenky, G., and Krueger, J.M. (2009). Physiological markers of local sleep. Eur. J. Neurosci. *29*, 1771–1778.
6. Borbély, A.A., and Achermann, P. (1992). Concepts and models of sleep regulation: an overview. J. Sleep Res. *1*, 63–79.
7. García-Marín, V., García-López, P., and Freire, M. (2007). Cajal's contributions to glia research. Trends Neurosci. *30*, 479–487.
8. Halassa, M.M., Florian, C., Fellin, T., Munoz, J.R., Lee, S.Y., Abel, T., Haydon, P.G., and Frank, M.G. (2009). Astrocytic modulation of sleep homeostasis and cognitive consequences of sleep loss. Neuron *61*, 213–219.
9. Pelluru, D., Konadhode, R.R., Bhat, N.R., and Shiromani, P.J. (2016). Optogenetic stimulation of astrocytes in the posterior hypothalamus increases sleep at night in C57BL/6J mice. Eur. J. Neurosci. *43*, 1298–1306.
10. Poskanzer, K.E., and Yuste, R. (2016). Astrocytes regulate cortical state switching in vivo. Proc. Natl. Acad. Sci. USA *113*, E2675–E2684.
11. Clasadonte, J., Scemes, E., Wang, Z., Boison, D., and Haydon, P.G. (2017). Connexin 43-mediated astroglial metabolic networks contribute to the regulation of the sleep-wake cycle. Neuron *95*, 1365–1380.e5.
12. Dani, J.W., Chernjavsky, A., and Smith, S.J. (1992). Neuronal activity triggers calcium waves in hippocampal astrocyte networks. Neuron *8*, 429–440.
13. Agulhon, C., Petravicz, J., McMullen, A.B., Sweger, E.J., Minton, S.K., Taves, S.R., Casper, K.B., Fiacco, T.A., and McCarthy, K.D. (2008). What is the role of astrocyte calcium in neurophysiology? Neuron *59*, 932–946.
14. Papouin, T., Dunphy, J.M., Tolman, M., Dineley, K.T., and Haydon, P.G. (2017). Septal cholinergic neuromodulation tunes the astrocyte-dependent gating of hippocampal NMDA receptors to wakefulness. Neuron *94*, 840–854.e7.
15. Durkee, C.A., and Araque, A. (2019). Diversity and specificity of astrocyte-neuron communication. Neuroscience *396*, 73–78.
16. Berridge, M.J., Lipp, P., and Bootman, M.D. (2000). The versatility and universality of calcium signalling. Nat. Rev. Mol. Cell Biol. *1*, 11–21.
17. Shigetomi, E., Patel, S., and Khakh, B.S. (2016). Probing the complexities of astrocyte calcium signaling. Trends Cell Biol. *26*, 300–312.
18. Bazargani, N., and Attwell, D. (2016). Astrocyte calcium signaling: the third wave. Nat. Neurosci. *19*, 182–189.
19. Verkhratsky, A., Orkand, R.K., and Kettenmann, H. (1998). Glial calcium: homeostasis and signaling function. Physiol. Rev. *78*, 99–141.
20. Fiacco, T.A., and McCarthy, K.D. (2006). Astrocyte calcium elevations: properties, propagation, and effects on brain signaling. Glia *54*, 676–690.
21. Verkhratsky, A., and Nedergaard, M. (2018). Physiology of astroglia. Physiol. Rev. *98*, 239–389.
22. Covelo, A., and Araque, A. (2018). Neuronal activity determines distinct gliotransmitter release from a single astrocyte. eLife *7*, e32237.
23. Frank, M.G. (2013). Astroglial regulation of sleep homeostasis. Curr. Opin. Neurobiol. *23*, 812–818.
24. Freeman, M.R. (2015). *Drosophila* central nervous system glia. Cold Spring Harb. Perspect. Biol. *7*, a020552.
25. Vorster, A.P., and Born, J. (2015). Sleep and memory in mammals, birds and invertebrates. Neurosci. Biobehav. Rev. *50*, 103–119.
26. Allada, R., and Siegel, J.M. (2008). Unearthing the phylogenetic roots of sleep. Curr. Biol. *18*, R670–R679.
27. Shaw, P.J., Cirelli, C., Greenspan, R.J., and Tononi, G. (2000). Correlates of sleep and waking in *Drosophila melanogaster*. Science *287*, 1834–1837.
28. Hendricks, J.C., Finn, S.M., Panckeri, K.A., Chavkin, J., Williams, J.A., Sehgal, A., and Pack, A.I. (2000). Rest in *Drosophila* is a sleep-like state. Neuron *25*, 129–138.
29. Vyazovskiy, V.V., Olcese, U., Lazimy, Y.M., Faraguna, U., Esser, S.K., Williams, J.C., Cirelli, C., and Tononi, G. (2009). Cortical firing and sleep homeostasis. Neuron *63*, 865–878.

(Right) Sleep amount over a 12-h period during (G) or 6 h after (H) dTrpA1 activation for *alrm-QF2 > QUAS-dTrpA1* (3^{rd}); *iso31 > UAS-TNT* (n = 54), *iso31 > QUAS-dTrpA1* (3^{rd}); *R72G06-GAL4 > UAS-TNT* (n = 46), and *alrm-QF2 > QUAS-dTrpA1* (3^{rd}); *R72G06-GAL4 > UAS-TNT* flies (n = 76) is shown. For (F)–(H), N = 3 independent trials, with similar results obtained for each trial.

(I) Model for astroglial Ca^{2+} signaling in the homeostatic regulation of sleep. Neural activity is increased during wakefulness and sensed by astrocytes, resulting in increased Ca^{2+} in the processes, which requires specific voltage-gated Ca^{2+} channels ("baseline"). Sleep loss generates protracted calcium signaling and leads to upregulation of TyrRII, sensitizing astrocytes to the actions of monoamines that are associated with wakefulness and further increasing Ca^{2+} levels in these cells ("priming"). When sufficient sleep need has accumulated, as measured by heightened levels of astroglial Ca^{2+}, transcription/translation of Spz is upregulated ("potentiated"). Spz is then released and acts on Toll receptors in the R5 neurons to promote global sleep drive.

See also Figures S6 and S7.

30. Ding, F., O'Donnell, J., Xu, Q., Kang, N., Goldman, N., and Nedergaard, M. (2016). Changes in the composition of brain interstitial ions control the sleep-wake cycle. Science *352*, 550–555.
31. Areal, C.C., Warby, S.C., and Mongrain, V. (2017). Sleep loss and structural plasticity. Curr. Opin. Neurobiol. *44*, 1–7.
32. Niethard, N., and Born, J. (2019). Back to baseline: sleep recalibrates synapses. Nat. Neurosci. *22*, 149–151.
33. Thomas, C.W., Guillaumin, M.C.C., McKillop, L.E., Achermann, P., and Vyazovskiy, V.V. (2020). Global sleep homeostasis reflects temporally and spatially integrated local cortical neuronal activity. eLife *9*, e54148.
34. Halassa, M.M., and Haydon, P.G. (2010). Integrated brain circuits: astrocytic networks modulate neuronal activity and behavior. Annu. Rev. Physiol. *72*, 335–355.
35. Losi, G., Mariotti, L., Sessolo, M., and Carmignoto, G. (2017). New tools to study astrocyte Ca2+ signal dynamics in brain networks *in vivo*. Front. Cell. Neurosci. *11*, 134.
36. Moeyaert, B., Holt, G., Madangopal, R., Perez-Alvarez, A., Fearey, B.C., Trojanowski, N.F., Ledderose, J., Zolnik, T.A., Das, A., Patel, D., et al. (2018). Improved methods for marking active neuron populations. Nat. Commun. *9*, 4440.
37. Liu, S., Liu, Q., Tabuchi, M., and Wu, M.N. (2016). Sleep drive is encoded by neural plastic changes in a dedicated circuit. Cell *165*, 1347–1360.
38. Saper, C.B., Fuller, P.M., Pedersen, N.P., Lu, J., and Scammell, T.E. (2010). Sleep state switching. Neuron *68*, 1023–1042.
39. Sehgal, A., and Mignot, E. (2011). Genetics of sleep and sleep disorders. Cell *146*, 194–207.
40. Weber, F., and Dan, Y. (2016). Circuit-based interrogation of sleep control. Nature *538*, 51–59.
41. Aston-Jones, G., and Bloom, F.E. (1981). Activity of norepinephrine-containing locus coeruleus neurons in behaving rats anticipates fluctuations in the sleep-waking cycle. J. Neurosci. *1*, 876–886.
42. Weinberg, Z.Y., and Puthenveedu, M.A. (2019). Regulation of G protein-coupled receptor signaling by plasma membrane organization and endocytosis. Traffic *20*, 121–129.
43. Ng, F.S., Sengupta, S., Huang, Y., Yu, A.M., You, S., Roberts, M.A., Iyer, L.K., Yang, Y., and Jackson, F.R. (2016). TRAP-seq profiling and RNAi-based genetic screens identify conserved glial genes required for adult *Drosophila* behavior. Front. Mol. Neurosci. *9*, 146.
44. Nagarkar-Jaiswal, S., DeLuca, S.Z., Lee, P.T., Lin, W.W., Pan, H., Zuo, Z., Lv, J., Spradling, A.C., and Bellen, H.J. (2015). A genetic toolkit for tagging intronic MiMIC containing genes. eLife *4*, e08469.
45. Ma, Z., Stork, T., Bergles, D.E., and Freeman, M.R. (2016). Neuromodulators signal through astrocytes to alter neural circuit activity and behaviour. Nature *539*, 428–432.
46. Bazargani, N., and Attwell, D. (2017). Amines, astrocytes, and arousal. Neuron *94*, 228–231.
47. Shang, Y., Griffith, L.C., and Rosbash, M. (2008). Light-arousal and circadian photoreception circuits intersect at the large PDF cells of the *Drosophila* brain. Proc. Natl. Acad. Sci. USA *105*, 19587–19594.
48. Parisky, K.M., Agosto, J., Pulver, S.R., Shang, Y., Kuklin, E., Hodge, J.J.L., Kang, K., Liu, X., Garrity, P.A., Rosbash, M., and Griffith, L.C. (2008). PDF cells are a GABA-responsive wake-promoting component of the *Drosophila* sleep circuit. Neuron *60*, 672–682.
49. Sheeba, V., Fogle, K.J., Kaneko, M., Rashid, S., Chou, Y.T., Sharma, V.K., and Holmes, T.C. (2008). Large ventral lateral neurons modulate arousal and sleep in *Drosophila*. Curr. Biol. *18*, 1537–1545.
50. Cao, G., and Nitabach, M.N. (2008). Circadian control of membrane excitability in *Drosophila melanogaster* lateral ventral clock neurons. J. Neurosci. *28*, 6493–6501.
51. Sheeba, V., Gu, H., Sharma, V.K., O'Dowd, D.K., and Holmes, T.C. (2008). Circadian- and light-dependent regulation of resting membrane potential and spontaneous action potential firing of *Drosophila* circadian pacemaker neurons. J. Neurophysiol. *99*, 976–988.
52. Liu, S., Lamaze, A., Liu, Q., Tabuchi, M., Yang, Y., Fowler, M., Bharadwaj, R., Zhang, J., Bedont, J., Blackshaw, S., et al. (2014). WIDE AWAKE mediates the circadian timing of sleep onset. Neuron *82*, 151–166.
53. Krueger, J.M., Nguyen, J.T., Dykstra-Aiello, C.J., and Taishi, P. (2019). Local sleep. Sleep Med. Rev. *43*, 14–21.
54. Hu, X., Yagi, Y., Tanji, T., Zhou, S., and Ip, Y.T. (2004). Multimerization and interaction of Toll and Spätzle in *Drosophila*. Proc. Natl. Acad. Sci. USA *101*, 9369–9374.
55. Lewis, M., Arnot, C.J., Beeston, H., McCoy, A., Ashcroft, A.E., Gay, N.J., and Gangloff, M. (2013). Cytokine Spatzle binds to the *Drosophila* immunoreceptor Toll with a neurotrophin-like specificity and couples receptor activation. Proc. Natl. Acad. Sci. USA *110*, 20461–20466.
56. Li, G., Forero, M.G., Wentzell, J.S., Durmus, I., Wolf, R., Anthoney, N.C., Parker, M., Jiang, R., Hasenauer, J., Strausfeld, N.J., et al. (2020). A Toll-receptor map underlies structural brain plasticity. eLife *9*, e52743.
57. Letellier, M., Park, Y.K., Chater, T.E., Chipman, P.H., Gautam, S.G., Oshima-Takago, T., and Goda, Y. (2016). Astrocytes regulate heterogeneity of presynaptic strengths in hippocampal networks. Proc. Natl. Acad. Sci. USA *113*, E2685–E2694.
58. Barres, B.A., Chun, L.L., and Corey, D.P. (1989). Calcium current in cortical astrocytes: induction by cAMP and neurotransmitters and permissive effect of serum factors. J. Neurosci. *9*, 3169–3175.
59. MacVicar, B.A. (1984). Voltage-dependent calcium channels in glial cells. Science *226*, 1345–1347.
60. Rungta, R.L., Bernier, L.-P., Dissing-Olesen, L., Groten, C.J., LeDue, J.M., Ko, R., Drissler, S., and MacVicar, B.A. (2016). Ca^{2+} transients in astrocyte fine processes occur via Ca^{2+} influx in the adult mouse hippocampus. Glia *64*, 2093–2103.
61. MacNamee, S.E., Liu, K.E., Gerhard, S., Tran, C.T., Fetter, R.D., Cardona, A., Tolbert, L.P., and Oland, L.A. (2016). Astrocytic glutamate transport regulates a *Drosophila* CNS synapse that lacks astrocyte ensheathment. J. Comp. Neurol. *524*, 1979–1998.
62. Lipscombe, D., Helton, T.D., and Xu, W. (2004). L-type calcium channels: the low down. J. Neurophysiol. *92*, 2633–2641.
63. Ingiosi, A.M., Hayworth, C.R., Harvey, D.O., Singletary, K.G., Rempe, M.J., Wisor, J.P., et al. (2020). A role for astroglial calcium in mammalian sleep. Curr. Biol. *30*, 1–11.
64. Bojarskaite, L., Bjørnstad, D.M., Pettersen, K.H., Cunen, C., Hermansen, G.H., Åbjørsbråten, K.S., Chambers, A.R., Sprengel, R., Vervaeke, K., Tang, W., et al. (2020). Astrocytic Ca^{2+} signaling is reduced during sleep and is involved in the regulation of slow wave sleep. Nat. Commun. *11*, 3240.
65. Bayliss, A., Roselli, G., and Evans, P.D. (2013). A comparison of the signalling properties of two tyramine receptors from *Drosophila*. J. Neurochem. *125*, 37–48.
66. O'Donnell, J., Ding, F., and Nedergaard, M. (2015). Distinct functional states of astrocytes during sleep and wakefulness: Is norepinephrine the master regulator? Curr. Sleep Med. Rep. *1*, 1–8.
67. Richter, C., Woods, I.G., and Schier, A.F. (2014). Neuropeptidergic control of sleep and wakefulness. Annu. Rev. Neurosci. *37*, 503–531.
68. Mackiewicz, M., Naidoo, N., Zimmerman, J.E., and Pack, A.I. (2008). Molecular mechanisms of sleep and wakefulness. Ann. N Y Acad. Sci. *1129*, 335–349.
69. Ingiosi, A.M., and Opp, M.R. (2016). Sleep and immunomodulatory responses to systemic lipopolysaccharide in mice selectively expressing interleukin-1 receptor 1 on neurons or astrocytes. Glia *64*, 780–791.
70. Cajochen, C., Brunner, D.P., Kräuchi, K., Graw, P., and Wirz-Justice, A. (1995). Power density in theta/alpha frequencies of the waking EEG progressively increases during sustained wakefulness. Sleep *18*, 890–894.
71. Gupta, C., López, J.M., Ott, W., Josić, K., and Bennett, M.R. (2013). Transcriptional delay stabilizes bistable gene networks. Phys. Rev. Lett. *111*, 058104.
72. Glass, L., Beuter, A., and Larocque, D. (1988). Time delays, oscillations, and chaos in physiological control systems. Math. Biosci. *90*, 111–125.

73. Ferrell, J.E., Jr. (2002). Self-perpetuating states in signal transduction: positive feedback, double-negative feedback and bistability. Curr. Opin. Cell Biol. *14*, 140–148.

74. Marucci, L., Barton, D.A.W., Cantone, I., Ricci, M.A., Cosma, M.P., Santini, S., di Bernardo, D., and di Bernardo, M. (2009). How to turn a genetic circuit into a synthetic tunable oscillator, or a bistable switch. PLoS ONE *4*, e8083.

75. Angeli, D., Ferrell, J.E., Jr., and Sontag, E.D. (2004). Detection of multistability, bifurcations, and hysteresis in a large class of biological positive-feedback systems. Proc. Natl. Acad. Sci. USA *101*, 1822–1827.

76. Brand, A.H., and Perrimon, N. (1993). Targeted gene expression as a means of altering cell fates and generating dominant phenotypes. Development *118*, 401–415.

77. Wang, Y., DelRosso, N.V., Vaidyanathan, T.V., Cahill, M.K., Reitman, M.E., Pittolo, S., Mi, X., Yu, G., and Poskanzer, K.E. (2019). Accurate quantification of astrocyte and neurotransmitter fluorescence dynamics for single-cell and population-level physiology. Nat. Neurosci. *22*, 1936–1944.

78. Thévenaz, P., Ruttimann, U.E., and Unser, M. (1998). A pyramid approach to subpixel registration based on intensity. IEEE Trans. Image Process. *7*, 27–41.

79. Pnevmatikakis, E.A., and Giovannucci, A. (2017). NoRMCorre: An online algorithm for piecewise rigid motion correction of calcium imaging data. J. Neurosci. Methods *291*, 83–94.

80. Friard, O., and Gamba, M. (2016). BORIS: a free, versatile open-source event-logging software for video/audio coding and live observations. Methods Ecol. Evol. *7*, 1325–1330.

81. Geissmann, Q., Garcia Rodriguez, L., Beckwith, E.J., French, A.S., Jamasb, A.R., and Gilestro, G.F. (2017). Ethoscopes: an open platform for high-throughput ethomics. PLoS Biol. *15*, e2003026.

82. Ryder, E., Blows, F., Ashburner, M., Bautista-Llacer, R., Coulson, D., Drummond, J., Webster, J., Gubb, D., Gunton, N., Johnson, G., et al. (2004). The DrosDel collection: a set of P-element insertions for generating custom chromosomal aberrations in *Drosophila melanogaster*. Genetics *167*, 797–813.

83. Hanesch, U., Fischbach, K.-F., and Heisenberg, M. (1989). Neuronal architecture of the central complex in *Drosophila melanogaster*. Cell Tissue Res. *257*, 343–366.

84. Lin, C.Y., Chuang, C.C., Hua, T.E., Chen, C.C., Dickson, B.J., Greenspan, R.J., and Chiang, A.S. (2013). A comprehensive wiring diagram of the protocerebral bridge for visual information processing in the *Drosophila* brain. Cell Rep. *3*, 1739–1753.

85. Omoto, J.J., Keleş, M.F., Nguyen, B.M., Bolanos, C., Lovick, J.K., Frye, M.A., and Hartenstein, V. (2017). Visual input to the *Drosophila* central complex by developmentally and functionally distinct neuronal populations. Curr. Biol. *27*, 1098–1110.

86. Doherty, J., Logan, M.A., Taşdemir, O.E., and Freeman, M.R. (2009). Ensheathing glia function as phagocytes in the adult *Drosophila* brain. J. Neurosci. *29*, 4768–4781.

87. Bellesi, M., de Vivo, L., Tononi, G., and Cirelli, C. (2015). Transcriptome profiling of sleeping, waking, and sleep deprived adult heterozygous Aldh1L1 - eGFP-L10a mice. Genom. Data *6*, 114–117.

88. Heiman, M., Kulicke, R., Fenster, R.J., Greengard, P., and Heintz, N. (2014). Cell type-specific mRNA purification by translating ribosome affinity purification (TRAP). Nat. Protoc. *9*, 1282–1291.

STAR★METHODS

KEY RESOURCES TABLE

REAGENT or RESOURCE	SOURCE	IDENTIFIER
Antibodies		
Rabbit polyclonal anti-GFP	Life technologies	Cat# A-11122
Chicken polyclonal anti-GFP	Life technologies	Cat# A-10262
Rabbit polyclonal anti-DsRed	Clontech/Fisher Scientific	Cat# NC9580775
Mouse monoclonal anti-brp	DSHB	RRID:AB_2314866
Alexafluor 488 anti-rabbit	Life technologies	Cat# A-11008
Alexafluor 488 anti-chicken	Life technologies	Cat# A-11039
Alexafluor 568 anti-mouse	Life technologies	Cat# A-11031
Mouse monoclonal anti-eGFP	Memorial Sloan Kettering Cancer Center	RRID:AB_2716737
Chemicals, Peptides, and Recombinant Proteins		
protease XIV	Sigma-Aldrich	Cat# P5147
Critical Commercial Assays		
Dynabeads Antibody Coupling Kit	Invitrogen	Cat# 14311D
SuperScript III RT Kit	Invitrogen	Cat# 18080085
Experimental Models: Organisms/Strains		
alrm-GAL4	Bloomington *Drosophila* Stock Center	Cat# 67032
alrm-QF2 (J)	Wu Lab	N/A
GMR58H05-AD	Wu Lab	N/A
GMR46C03-DBD	Wu Lab	N/A
GMR58H05-QF2 (7)	Wu Lab	N/A
GMR72G06-GAL4	Bloomington *Drosophila* Stock Center	Cat# 39792
GMR86E01-GAL4	Bloomington *Drosophila* Stock Center	Cat# 45914
Iso31	Bloomington *Drosophila* Stock Center	Cat# 5905
LexAop2-CD2::GFP	Bloomington *Drosophila* Stock Center	Cat# 66687
Pdf-GAL4	Bloomington *Drosophila* Stock Center	Cat# 6900
Pdf-LexA	Gift from M. Rosbash	N/A
QUAS-dTrpA1 (2nd)	Gift from C. Potter	N/A
QUAS-dTrpA1 (3rd)	Gift from C. Potter	N/A
QUAS-GCaMP6s	Gift from C. Potter	N/A
QUAS-mtdTomato::3xHA	Bloomington *Drosophila* Stock Center	Cat# 80905
UAS-IVS-jGCaMP7s	Bloomington *Drosophila* Stock Center	Cat# 30005
UAS-CD4::tdTomato	Bloomington *Drosophila* Stock Center	Cat# 35837
Mi{PT-GFSTF.2}TyrRII$^{MI12699\text{-}GFSTF.2}$	Bloomington *Drosophila* Stock Center	Cat# 65339
UAS-Ca alpha 1D RNAi #1	Bloomington *Drosophila* Stock Center	Cat# 25830
UAS-Ca alpha 1D RNAi #2	Bloomington *Drosophila* Stock Center	Cat# 33413
UAS-CaMPARI2 (L398T)	Gift from E. Schreiter	N/A
UAS-dTrpA1^{attp18}	Gift from G. Rubin	N/A
UAS-dTrpA1^{attp16}	Bloomington *Drosophila* Stock Center	Cat# 26263
UAS-mCD8::GFP	Bloomington *Drosophila* Stock Center	Cat# 5137
UAS-mCD4::tdTomato	Bloomington *Drosophila* Stock Center	Cat# 35837
UAS-myr-GCAMP6s	Gift from T. Littleton	N/A
UAS-RNAi (various)	Harvard Transgenic RNAi Project	See Table S1
UAS-RNAi (various)	Vienna *Drosophila* Resource Center	See Table S1
UAS-Rpl10a::EGFP	Bloomington *Drosophila* Stock Center	Cat# 42683
UAS-Spz RNAi #1	Bloomington *Drosophila* Stock Center	Cat# 34699

(*Continued on next page*)

Continued

REAGENT or RESOURCE	SOURCE	IDENTIFIER
UAS-Spz RNAi #2	Vienna *Drosophila* Resource Center	Cat# 105017
UAS-TNT	Bloomington *Drosophila* Stock Center	Cat# 28838
UAS-Toll-miR (B)	Wu Lab	N/A
UAS-Toll-RNAi #1	Bloomington *Drosophila* Stock Center	#35628
UAS-TyrRII RNAi #1	Bloomington *Drosophila* Stock Center	#64964
UAS-TyrRII RNAi #2	Vienna Drosophila Resource Center	#110525
UAS-wtrw (2.23)	Gift from M. Freeman	N/A
Oligonucleotides		
ATT ACC ATG CTG GAC CGG GTG CAA GG	IDT	GMR58H05-F
CTC ACA AGT CAT GGC CCT AAC GAG G	IDT	GMR58H05-R
GAT CGA TCG CGG CCG CTA GTG GCG ATC CTT TCG CTC G	IDT	*alrm*-F
GAT CGG TAC CGA GTT AAT ATG GTG GGA ACT GC	IDT	*alrm*-R
GAT CAA AGT TTG GGG CAA CTA CCC T	IDT	GMR46C03-F
GGT TCC CGC AAA GTT AAT CTC CTG T	IDT	GMR46C03-R
TCT CGA ACT AAG GGC AAA TAT C	IDT	Toll-miR 1st
GGC GAG GGC TAC AAC AAT AAT C	IDT	Toll-miR 2nd
GCA TCA AGA AGA AGA AGA CGA GA	IDT	*repo*-F
GTT CAA AGG CAC GCT CCA	IDT	*repo*-R
GGT CGA TGA GGT CGT GGA C	IDT	*nSyb*-F
CCA GAA TTT CCT CTT GAG CTT GC	IDT	*nSyb*-R
CGG ATC GAT ATG CTA AGC TGT	IDT	*Rpl49*-F
CGA CGC ACT CTG TTG TCG	IDT	*Rpl49*-R
GCA ACG ATC TTC AGC CCA CG	IDT	*spz*-F
TTG ATC CGC TCC TTC GCA CT	IDT	*spz*-R
GGC TGG ATA CTG TGC GAC AT	IDT	TyrRII-F
GTG ACG GCG AGA TAC CTG TC	IDT	TyrRII-R
Recombinant DNA		
pUAST	[76]	N/A
pPTQF#7-hsp70	Addgene	Cat# 46136
pBPp65ADZpUw	Addgene	Cat# 26234
pBPZpGAL4DBDUw	Addgene	Cat# 26233
Software and Algorithms		
AQuA	[77]	N/A
Fiji	*Open Source*	RRID:SCR_002285
TurboReg ImageJ Plugin	[78]	*N/A*
Custom ImageJ Macros	Wu Lab	https://github.com/marknwulab/Blum-et-al.-2020
Motion Correction Software for *In vivo* calcium imaging	[79]	N/A
Behavioral Observation Research Interactive Software (Boris)	[80]	N/A
rethomics	[81]	N/A
MATLAB	Mathworks	RRID:SCR_001622
Custom MATLAB Scripts	Wu Lab	https://github.com/marknwulab/Blum-et-al.-2020
Axon pClamp11	Molecular Devices	RRID:SCR_011323
Prism 7	Graphpad	RRID:SCR_002798
PrairieView Software	Bruker	RRID:SCR_017142
DAMSystem308	Trikinetics	RRID:SCR_016191
DAMFileScan111	Trikinetics	N/A

(*Continued on next page*)

Continued

REAGENT or RESOURCE	SOURCE	IDENTIFIER
Zen Black	Zeiss	RID:SCR_013672
Zen Blue	Zeiss	RID:SCR_013672
Other		
Glass Bottom Petri Dishes	Pelco	Cat# 14035-20
DAM2 Activity Monitors	Trikinetics	Cat# DAM2
LC-4 Light Controller	Trikinetics	Cat# LC4
PSIU9 Power Supply Interface	Trikinetics	Cat# PSIU9
Vortexer with Vortex Mounting Plate	Trikinetics	Cat# TVOR-120
Laser cut adaptor plate for vortexer	Wu Lab	https://github.com/marknwulab/Blum-et-al.-2020
LCS-1 Heat Exchanger	Warner Instruments	Cat# 64-1922
CL-100 Single Channel Bipolar Temp Controller	Warner Instruments	Cat# 64-0352
SC-20 In-line Heater/Cooler	Warner Instruments	Cat# 64-0353
ThermoClamp-01	Automate Scitentific	Cat# 03-11-LL
Scientifica Temperature Controller	Scientifica	Cat# SM-4500
Syringe Filter (0.22 μm)	Thermo Fisher	Cat# 09-926-3
UV Curing Glue	Loctite	Cat# 3972
Opticure LED 200	Norland	Cat# LED 200

RESOURCE AVAILABILITY

Lead Contact

Further information and requests for resources and reagents should be directed to and will be fulfilled by the Lead Contact, Dr. Mark N. Wu (marknwu@jhmi.edu).

Materials Availability

Transgenic *Drosophila* strains generated for this manuscript are available upon request to lead contact.

Data and Code Availability

The datasets supporting the current study are available from the lead contact upon reasonable request. MATLAB algorithms and ImageJ macros can be accessed freely in our lab Github repository (https://github.com/marknwulab/Blum-et-al.-2020).

EXPERIMENTAL MODEL AND SUBJECT DETAILS

Drosophila melanogaster adult females (~4-10 days old) were employed in all studies.

METHOD DETAILS

Fly Stocks and maintenance

Flies were maintained on standard food containing molasses, cornmeal, and yeast at room temperature. Mated female flies back-crossed at least 5 generations against the *iso31* strain or generated in the *iso31* background[82] were used for all experiments. All crosses and stocks were reared in a12hr:12hr light/dark cycle and maintained at 25°C for all experiments except those containing the *UAS-dTrpA1* transgene (or associated controls) which were maintained at 23°C to avoid premature thermogenetic activation prior to experimentation. Please see the Key Resources Table for nomenclature, genotypes and sources for fly strains used.

Nomenclature

Because two different groups of ellipsoid body (EB) rings neurons have been named "R2" neurons,[83,84] for clarity we have adopted the EB ring nomenclature outlined by Omoto et al.[85] and refer to the sleep drive neurons we previously characterized[37] as "R5" neurons.

Molecular Biology

The *alrm-QF2* and *R58H05-QF2* lines were generated by subcloning the *alrm* enhancer region[86] and the GMR58H05 enhancer, respectively, into pPTQF#7-hsp70 (Addgene# 46136) using EcoRI and BamHI. The *R58H05-AD* and *R46C03-DBD* lines were

generated by subcloning their respective enhancer regions into pBPp65ADZpUw (Addgene# 26234) or pBPZpGAL4DBDUw (Addgene# 26233), using Gateway cloning (Thermo Fisher). The following primers were used for PCR amplification of enhancers: *R58H05-F* 5′ - ATT ACC ATG CTG GAC CGG GTG CAA GG - 3′; *R58H05-R* 5′ - CTC ACA AGT CAT GGC CCT AAC GAG G - 3′; *alrm-F* 5′ - GAT CGA TCG CGG CCG CTA GTG GCG ATC CTT TCG CTC G - 3′; *alrm-R* 5′ - GAT CGG TAC CGA GTT AAT ATG GTG GGA ACT GC - 3′; *R46C03-F* 5′ - GAT CAA AGT TTG GGG CAA CTA CCC T - 3′; and *R46C03-R* 5′ - GGT TCC CGC AAA GTT AAT CTC CTG T - 3′. The construct for *UAS-Toll-miR* was generated as previously described.[52] Two 22mers bridging the 1st and 2nd coding exons of the neural transcript of the *Toll* gene (TCT CGA ACT AAG GGC AAA TAT C and GGC GAG GGC TAC AAC AAT AAT C) were used to create the two hairpin loops. The entire microRNA construct was synthesized *in vitro* (GeneArt) and then subcloned into pUAST[76] using EcoRI and NotI. Transgenic lines were generated in the *iso*31 background either through P-element mediated random insertion (*alrm-QF2* and *UAS-Toll-miR*) or site-directed PhiC31-mediated insertion into the *86Fb* (*R58H05-AD*) and *vk27* (*R46C03-DBD*) insertion sites (Rainbow Transgenics).

Behavioral Analyses

Baseline sleep measurements

Sleep data collection was performed as previously described.[52] All analysis was performed using custom MATLAB scripts (Mathworks) according to previously established algorithms.[37] Briefly, CO_2-anesthetized 3-4 day old female flies were loaded into 5x65mm diameter glass tubes with 5% sucrose in agar and sealed with wax and yarn, and then allowed to recover for ~1.5 days prior to data collection. Flies were loaded into *Drosophila* Activity Monitoring System devices (DAMS, Trikinetics), which were placed in incubators at 22°C with independent lighting control (12 hr:12 hr L:D cycles). Sleep was identified based on the previously established criterion of 5 contiguous min of locomotor activity quiescence.[27] A sleep bout was defined as a $\geq$ 5 contiguous min period of locomotor quiescence bounded by locomotor activity on both sides.

Thermogenetic activation

Unless otherwise specified, *UAS-dTrpA1* on the 2nd chromosome was used for thermogenetic activation experiments, and activation was performed by ramping the temperature of the incubator according to the schedules described herein. Continuous temperature monitoring revealed an ~30 min lag for temperatures to stably reach desired setpoints, which is reflected in the times used for analysis of sleep during activation for the 1 hr pulse (i.e., ZT0.5-ZT1.5).

Mechanical sleep deprivation

Flies were mechanically stimulated for 2-10 s/min from ZT12-ZT24 using a vortexer mounting plate and multi-tube vortexer (Trikinetics). Only data from flies with $\geq$ 90% reduction in sleep amount during deprivation, compared with baseline conditions, were included for analysis. "% Sleep Recovered" was calculated by using a sliding 30 min window to subtract baseline sleep from post-deprivation sleep binwise and then summing each with all previous bins to provide a cumulative tally of sleep time over the twelve hours post-deprivation. We then divided each 30 min bin by the total sleep lost (nighttime sleep during baseline – nighttime sleep during deprivation) and converted this ratio to a percentage.

Arousal threshold analysis

Flies were mechanically stimulated for 1 s/hr from ZT15-ZT21 and again from ZT1-ZT7 using a vortexer mounting plate and multi-tube vortexer (Trikinetics). The intensity of stimulus was varied using the speed adjustment knob of the vortexer from 1 (mild) to 3 (moderate) to 7 (strong) with two consecutive hourly pulses at each respective intensity, in that order. These brief arousals were performed with concomitant overnight thermogenetic activation (28°C) from ZT12-24 and a return to baseline temperatures from ZT0-12 (22°C). Flies that were inactive for 5 min before a stimulus and exhibited beam crossings within 3 min after the mechanical stimulus were identified as "aroused" and where possible the two repeats for each animal at each intensity and temperature condition were averaged. The percentage was calculated as the number of animals aroused compared to all potentially arousable animals (i.e., inactive for 5 min prior to stimulus) and each experiment was performed in triplicate.

RNAi screens

For the Ca^{2+} effector miniscreen, we identified genes encoding proteins that flux Ca^{2+}, including ionotropic receptors, channels, transporters, and exchangers. *UAS-RNAi* lines for these genes were crossed to *R86E01-GAL4*, and the appropriate progeny (n = 8) were assessed for sleep rebound phenotypes following mechanical SD from ZT12-ZT24. Sleep rebound was calculated as the difference in sleep amount from ZT0-6 post-deprivation compared to ZT0-6 the day prior. For our large-scale screen ~3,200 *UAS-RNAi* lines were selected for genes that were either randomly selected or identified from previous mammalian and invertebrate astrocyte expression studies.[43,87] These *UAS-RNAi* lines were crossed to *alrm-GAL4>UAS-dTrpA1* flies, and the appropriate progeny (n = 4) were assessed for "rebound" sleep phenotypes for the 6 hr following a 1 hr 31°C heat pulse from ZT0-1. This parameter was defined as the difference in sleep from ZT1-7 post-activation compared to ZT1-7 the day prior, calculated for each individual before averaging. Lines exhibiting sleep parameters $\geq$ 2.5 SD less than the mean were selected for secondary screening and further characterization.

Video analysis

Flies were loaded into 3D-printed Raspberry Pi-enabled recording chambers (Ethoscopes) and recorded using high-resolution video mode.[81] After two baseline days for acclimatization, the animals were recorded for 2 hr during thermogenetic activation (ZT 20-22, 28°C) and 2 hr after activation (ZT 2-4, 22°C). The first hour of each recording was used for manual scoring of behavior using open-source Behavioral Observation Research Interactive Software (BORIS).[80] Behaviors were categorized into 4 possible states each minute. In cases where multiple behaviors were observed within the same minute, they were classified in this

order: feeding > grooming > locomotion > immobility such that only the highest order state was labeled regardless of the presence of the other behavioral states.

Imaging

Confocal Microscopy

All confocal images were acquired from coverslipped (size 1.5) and Vectashield (Vector Labs) mounted samples using an LSM710 microscope and Zen Black image capture software (Zeiss International), except for CaMPARI and super-resolution images which were performed on an inverted LSM800 fitted with Airyscan detectors. In the latter case, Airyscan detectors were calibrated to the brightest signal from the experimental condition and then these settings were used for all samples. In all cases, pinhole aperture and slice thickness were optimized according to the software recommendations for lens NA, magnification, and reported XY resolution.

Ex vivo CaMPARI imaging

4-5 day old flies were loaded into locomotor tubes for sleep recordings ± mechanical deprivation (as described above). Animals were removed between ZT0-ZT3 or ZT12-15 and quickly dissected in sterile filtered (0.22 μm) Adult Hemolymph-Like Saline (AHLS, 103 mM NaCl, 3 mM KCl, 1.5 mM $CaCl_2$, 4 mM $MgCl_2$, 26 mM $NaHCO_3$, 1 mM NaH_2PO_4, 10 mM trehalose, 10 mM glucose, 5 mM TES Buffer, 2 mM sucrose) and then transferred to glass bottomed dishes (Pelco, 14035-20). Data were collected as 1024x1024 pixel confocal stacks targeting approximately 10 μm thick slices of the Antennal Lobes (AL) and Superior Medial Lobes (SMP) centered on astrocyte cell bodies using a 63X lens (Zeiss Plan-Apochromat 63x/1.4 Oil) prior to, and immediately after, photoconversion (PC) using 20% intensity light generated by a TTL LED (Excite) filtered with a 395/25 nm bandpass filter. Photoconversion was achieved by quickly cycling the LED with a 500ms/200ms duty cycle performed for 240 cycles (~2.8 minutes total). Data were analyzed by first applying the "TurboReg" plugin[78] of ImageJ (NIH) to align pre- and post-PC images and then manually drawing ROIs covering individual astrocyte cell bodies and a single neuropil region using the green channel of pre-PC images. Data analyses and generation of heat-mapped images were performed with a custom macro written for ImageJ by first performing maximal intensity projection and then applying the photoconversion algorithm used by Moeyaert et al., 2018.[36] Briefly, "Fold R/G" for images represent $(Red/Green)_{post}$ divided by $(Red/Green)_{pre}$ at the pixel level. Average Fold R/G across each ROI was used for quantification.

Immunocytochemistry

Immunostaining of whole-mount brains was performed as previously described.[37] Briefly, brains were fixed in 4% PFA for ~30 min, washed 5x in PBST (PBS + 0.3% Triton X-100), then blocked in normal goat serum, before incubation with rabbit anti-GFP (Invitrogen, 1:1000), chicken anti-GFP (Invitrogen, 1:200), rabbit anti-DsRed (Clontech, 1:1000), or mouse anti-brp (nc82, Development Studies Hybridoma Bank, 1:20), at 4°C for ~48 hr, followed by incubation with Alexa 488 anti-rabbit (Invitrogen, 1:1000), Alexa 488 anti-chicken (Invitrogen, 1:1000), or Alexa 568 anti-mouse (Invitrogen, 1:1000) secondary antibodies at 4°C for 2-24 hr.

TyrRII::GFP quantification

Data were collected from flies expressing GFP-tagged Tyramine Receptor II as 1024x1024 pixel confocal stacks using a 40x lens (Zeiss Plan-Apochromat 40x/1.3 Oil) and were cropped to include the AL. Stacks were processed and calculated using a custom macro written for ImageJ using "Maximum Entropy Thresholding" and the "Analyze Particles" function with a 3-100 pixel cutoff to quantify GFP puncta.

In vivo astrocyte GCaMP imaging

5-6 day old flies were anesthetized on ice and placed in a hole that was etched on a stainless steel shim attached to a custom 3D-printed holder. The head capsule and thorax were glued to the shim using UV cured glue (Loctite, 3972). Legs, proboscis and antennae were immobilized using beeswax applied with a heated metal probe. The head capsule was bathed in AHLS. A small window was opened by removing the cuticle above the central brain using sharpened forceps (Dumont 5SF). Fat and other tissue were removed to gain optical access to the brain. Astrocytes expressing myristoylated GCaMP6s were imaged using 2-photon microscopy from ZT0-2 with a Zeiss LSM 710 microscope using a Ti:Sapphire Laser (@920nm, Chameleon Ultra II, Coherent). Images were acquired at 0.484 s a frame (~2.1 Hz). The image window was 80 × 80 μm at 256 × 256 pixel resolution, and duration of imaging did not exceed 8 min per animal. The imaging plane was limited to the superior medial protocerebrum (SMP). Animals exhibiting spontaneous astrocytic Ca^{2+} activity were analyzed. Acquired images were first motion-corrected using a previously published method[79] with custom parameters. Motion-corrected images were analyzed using AQuA (Astrocyte Quantitative Analysis) which allows characterization of spatiotemporally distinct events.[77] Events were identified based on empirically determined parameters, which were applied to all images. Traces from each event were exported and filtered with a 3rd order Savitzky-Golay filter over 15 frames.

Ellipsoid body R5 ring GCaMP imaging

Astrocyte thermogenetic activation: For intracellular Ca^{2+} measurements of the R5 ellipsoid body ring, 5-6 day old *R58H05-QF2 > QUAS-GCAMP6s, QUAS-mtdTomato-3xHA* flies bearing either *alrm-GAL4 > UAS-dTrpA1 or UAS-dTrpA1* alone transgenes were examined. All animals were administered a heat stimulus (31°C) from ZT0-ZT1 and dissected and imaged from ZT3-ZT5. Brains were quickly dissected in calcium free AHLS (0 mM $CaCl_2$, 5.5 mM $MgCl_2$) and then transferred to a sample chamber containing room temperature AHLS (as described above) and imaged using an Ultima multiphoton microscope (Prairie Technologies). Excitation of both GCaMP6s and mtdTomato was achieved with 920nm light produced by a Ti:Sapphire Laser (Chameleon Ultra II, Coherent). Data were collected using a 40x water immersion lens with 2x optical detector zoom (Olympus LUMPLFLN 40XW/0.8) as a single 512x512 pixel plane over 60 s at a frequency of ~1 Hz using Prairieview software (Prairie Technologies). The imaging plane was

selected based on the completeness of the R5 ring which sits almost perpendicular to the dorsal surface of the fly brain. Data were analyzed using ImageJ to calculate the mean intensity of the R5 ring targeting ROIs (after calculating pixel by pixel GCaMP/mtdTomato ratios) and then averaging over the full recording.

Mechanical deprivation and Toll knockdown

For intracellular Ca^{2+} measurements of the R5 ellipsoid body ring, 5-6 day old *R58H05-Gal4 > UAS-GCAMP7s, UAS-CD4:tdTomato* flies were used with some animals additionally carrying the UAS-Tl miR transgene in order to knockdown Toll expression specifically within the R5 ring. All animals were loaded into standard locomotor tubes for four days prior to being dissected and imaged from ZT3-5. While "no SD" controls received no other manipulation, both "SD" and "SD + Toll miR" flies were additionally exposed to 24hrs of sleep deprivation (using mechanical stimulation at a frequency of 6 s/min as described above) prior to collection on the third day. Samples were prepared similarly to the thermogenetic activation experiment described above; however, we chose to increase the spatial resolution and capture Ca^{2+} dynamics across the entire ring structure. Therefore, we used a modified protocol whereby the 40x water immersion lens was used with 4.02X optical detector zoom and coupled with a piezo stepper motor (for Z axis control) to collect approximately 18-20 slices with a 2 um step size across the entire ring structure (~40 um), and a resonant galvo scanning head to scan an entire volume every ~3 s at a resolution of 512x512 pixels per slice. The entire volume was scanned for 5 minutes. Data were analyzed using ImageJ by first calculating the maximum intensity projection of all slices in a single volume, then calculating the mean intensity of the R5 ring targeting ROIs over the entire recording (after calculating pixel by pixel GCaMP/mtdTomato ratios).

Electrophysiology

3 to 9 day old flies were used in whole-cell patch clamp and cell-attached recordings. Whole-cell patch clamp recordings were generally performed as described previously.[52] For sleep deprivation experiments, flies were dissected from ZT0-2 following either 12 hr baseline sleep or 12 hr of mechanical SD (from ZT12-ZT24) as described above or by using the ethoscope tracking system,[81] and whole-cell patch clamp recordings were performed using current-clamp mode. For astrocyte activation experiments, either whole-cell or cell-attached patch-clamp recordings were performed using current-clamp mode. Brains were dissected and recordings were performed in a *Drosophila* physiological saline solution (101 mM NaCl, 3 mM KCl, 1 mM $CaCl_2$, 4 mM $MgCl_2$, 1.25 mM NaH_2PO_4, 20.7 mM $NaHCO_3$, and 5 mM glucose [pH 7.2]), pre-bubbled with 95% O_2 and 5% CO_2, at room temperature. If needed for removal of the glial sheath, brains were treated with 2 mg/ml protease XIV (Sigma-Aldrich) for 5–8 min at 22°C. For both whole-cell and cell-attached recordings, l-LNvs were located using GFP fluorescence or infrared-differential interference contrast (IR-DIC) optics, under a fixed-stage upright microscope (BX51WI; Olympus or SliceScope, Scientifica). Patch-pipettes (5–13 MΩ) were made from borosilicate glass capillary with a Flaming- Brown puller (P-1000 or P-97; Sutter Instrument) and polished with a microforge. For whole-cell recordings, the pipette was filled with internal solution containing 102 mM potassium gluconate, 0.085 mM $CaCl_2$, 0.94 mM EGTA, 8.5 mM HEPES, 17 mM NaCl (pH 7.2), 4 mM Mg-ATP, and 0.5 mM Na-GTP. For cell-attached recordings, the pipette was filled with the filtered *Drosophila* physiological saline solution. For astrocyte dTrpA1 activation experiments heat stimulation was applied by perfusing solution that was preheated using a temperature controller (ThermoClamp-01, Automate Scientific, Berkeley, CA or Scientifica Temperature Controller, Scientifica) into the recording chamber. Recordings were acquired with an Axopatch 200B or Multiclamp 700B amplifier (Molecular Devices) and Digidata 1440A or Digidata 1550B interface (Molecular Devices), using pCLAMP 10 or 11. Signals were sampled at 10 or 20 kHz and low-pass filtered at 2 or 3 kHz. For each cell-attached recording, a brief electrical stimulus (15V amplitude, 10k Hz square wave, 0.05 ms duration) was applied after current-clamp recordings from each cell to verify access to the cell. The cell was discarded if this stimulus did not elicit action potentials. For the cell-attached recordings, 2 cells with a mean firing rate > 9 Hz were excluded, due to concerns about cell health.

Translating ribosomal affinity purification with quantitative polymerase chain reaction

Translating ribosomal affinity purification (TRAP) was performed as previously described using purified EGFP antibody (19C8 antibody, Memorial Sloan Kettering Cancer Center)[88] to pulldown ribosomal complexes and their associated transcripts. Briefly, ~1,024 fly heads (per group) were collected in liquid N_2 from 5-6 day old *R86E01-GAL4 > UAS-Rpl10a::EGFP* flies at ZT0-2 under baseline conditions or immediately following 12 hr mechanical SD from ZT12-ZT24 (described above). Following short-term storage at −80°C, heads were pulverized in homogenization buffer and then incubated with antibody-coupled magnetic beads (Dynabeads Antibody Coupling Kit, Invitrogen) to immunoprecipitate ribosomal bound mRNA species. After RNA extraction (Trizol, Invitrogen), cDNA libraries were synthesized using SuperScript III high capacity Reverse Transcription Kit (Invitrogen), and qPCR was performed using the Power SYBR Green PCR master mix (Life Technologies) using the following primers: *repo-F* 5′- GCA TCA AGA AGA AGA CGA GA – 3′; *repo-R* 5′- GTT CAA AGG CAC GCT CCA - 3′; *nSyb-F* 5′- GGT CGA TGA GGT CGT GGA C – 3′; *nSyb-R* 5′- CCA GAA TTT CCT CTT GAG CTT GC −3′; *Rpl49-F* 5′- CGG ATC GAT ATG CTA AGC TGT - 3′; *Rpl49-R* 5′- CGA CGC ACT CTG TTG TCG - 3′; *spz-F* 5′- GCA ACG ATC TTC AGC CCA CG – 3′; *spz-R* 5′- TTGATCCGCTCCTTCGCACT −3′; *TyrRII-F* 5′ – GGC TGG ATA CTG TGC GAC AT – 3′; *TyrRII-R* 5′- GTG ACG GCG AGA TAC CTG TC – 3′. A similar protocol was followed for the thermogenetic activation experiments instead using *alrm-QF2 > QUAS-dTrpA1; R86E01-GAL4 > UAS-Rpl10a::EGFP* or *iso*31 > *QUAS-dTrpA1; R86E01-GAL4 > UAS-Rpl10a::EGFP* at ZT0-2 immediately following overnight (ZT12-24) heat pulse at 28°C.

QUANTIFICATION AND STATISTICAL ANALYSIS

All analyses were performed using Prism 7 (Graphpad). Normally distributed data were analyzed using parametric tests (Student's t tests and one-way or two-way ANOVAs followed by Tukey's post hoc test) and plotted as bar graphs ± SEM, whereas data that violated the assumption of normality were analyzed using non-parametric tests (Kruskal-Wallis test followed by Dunn's post hoc test) and plotted as simplified boxplots (Median with 1st, and 3rd Quartile boxes). For the video analysis, a Chi-square analysis was performed to assess differences in the distribution of experimental *alrm>dTrpA1* group relative to expected values provided by the *UAS-dTrpA1*controls. For all statistical details such as p values, number of trials (N), and number of subjects (n), please see figure captions.